

Reconfigurable Intelligent Surface Enabled Full-Duplex/Half-Duplex Cooperative Non-Orthogonal Multiple Access

Mohamed Elhattab, *Student Member, IEEE*, Mohamed Amine Arfaoui, *Student Member, IEEE*, Chadi Assi, *Fellow, IEEE*, Ali Ghrayeb, *Fellow, IEEE*

Abstract

This paper investigates the downlink transmission of reconfigurable intelligent surface (RIS)-aided cooperative non-orthogonal-multiple-access (C-NOMA), where both half-duplex (HD) and full-duplex (FD) relaying modes are considered. The system model consists of one base station (BS), two users and one RIS. The goal is to minimize the total transmit power at both the BS and at the user-cooperating relay for each relaying mode by jointly optimizing the power allocation coefficients at the BS, the transmit power coefficient at the relay user, and the passive beamforming at the RIS, subject to power budget constraints, the successive interference cancellation constraint and the minimum required quality-of-service at both cellular users. To address the high-coupled optimization variables, an efficient algorithm is proposed by invoking an alternating optimization approach that decomposes the original problem into a power allocation sub-problem and a passive beamforming sub-problem, which are solved alternately. For the power allocation sub-problem, the optimal closed-form expressions for the power allocation coefficients are derived. Meanwhile, the semi-definite relaxation approach is exploited to tackle the passive beamforming sub-problem. The simulation results validate the accuracy of the derived power control closed-form expressions and demonstrate the gain in the total transmit power brought by integrating the RIS in C-NOMA networks.

Index Terms

C-NOMA, FD, HD, passive beamforming, power allocation, RIS, 6G.

Mohamed Elhattab is with the ECE Department, Concordia University, Montreal, Quebec, H3G 1M8, Canada (email: m_elhatt@encs.concordia.ca). Mohamed Amine Arfaoui and Chadi Assi are with the CIISE Department, Concordia University, Montreal, Quebec, H3G 1M8, Canada (email: m_arfaou@encs.concordia.ca, assi@mail.concordia.ca). Ali Ghrayeb is with the Electrical and Computer Engineering (ECE) department, Texas A & M University at Qatar, Doha, Qatar (e-mail: ali.ghrayeb@qatar.tamu.edu).

I. INTRODUCTION

A. Motivation

With the proliferation of numerous burgeoning applications and services such as ultra-reliable low-latency communication (URLLC), massive machine type communications (mMTC), enhanced mobile broadband (eMBB), among others, wireless communication systems are expected to face daunting challenges [1]. To satisfy and accommodate these ever-increasing traffic demands, the diverse quality-of-services (QoS) requirements, and the massive connectivity accompanied with these new applications, various innovative and promising technologies and architectures will need to be developed [2]. Novel multiple-access-techniques are currently being explored in both academia and industry lately [3] in order to accommodate for such unprecedented requirements.

Non-orthogonal multiple access (NOMA) has been deemed as one of the vital enabling multiple access techniques for the upcoming sixth-generation (6G) cellular networks [1], [4]. This is due to its ability of enhancing the network spectral efficiency and supporting massive number of connected devices [1]. NOMA has been included in the third Generation Partnership Project (3GPP) LTE-A standard (Release 15) [5].¹ Different from the traditional orthogonal multiple access (OMA) techniques, NOMA allows multiple user equipment (UEs) to utilize the same resource (radio frequency, time slot, code, etc.). This can be achieved by using superposition coding at the transmitter with appropriately power allocation coefficients and performing successive interference cancellation (SIC) at the receiver side to remove the intra-NOMA user interference [4]. This allows the UEs with poor channel conditions, which are referred to as “far” NOMA UEs, to be simultaneously served with the UEs that have good channel conditions, which are referred to as “near” NOMA UEs. It has been proven that NOMA achieves a significant gain over OMA techniques [6], [7].

With the objective of further enhancing the performance of NOMA cellular systems, the integration of user-cooperative relaying and NOMA, which is known as cooperative NOMA (C-NOMA), has been proposed [8]. In this transmission technique, with the aid of device-to-device (D2D) communication and the half-duplex (HD)/full-duplex (FD) relaying modes, the near NOMA UEs act as decode-and-forward (DF) relays for the far NOMA UEs. Specifically, the near NOMA UEs exploit the successive decoding strategy adopted at their sides to assist the transmissions between the BS and the far NOMA UEs [9], [10]. As a result, by adding the cooperation link between the near NOMA UEs and the far NOMA UEs as a new degree of diversity with the BS-UE links, C-NOMA based

¹The focus of this paper is on power domain NOMA, and thus, throughout this paper, the term NOMA is used to refer to power domain NOMA, unless otherwise stated.

cellular network can achieve higher spatial diversity and better fairness than NOMA [9]. While NOMA/C-NOMA transmission techniques are expected to unleash the potential of next-generation cellular networks, another new degree of freedom can be added to the network by making the wireless propagation environment controllable and programmable, which can be achieved through the reconfigurable intelligent surface (RIS) technology [11].

RIS has recently been recognized as a key promising technology for achieving cost-, energy-, and spectral-efficient communications via intelligently reconfiguring and controlling the wireless propagation environment [12], [13]. It is composed of a large number of passive low-cost elements, each of which is capable of independently tuning the phase-shift of the incident radio waves. For instance, by appropriately configuring the phase-shifts with the aid of the RIS controller, the reflected signals can be made to add constructively at the receiver, and therefore, enhancing the received signal strength at the point of interest. In contrast to traditional relays, RIS has the benefit of low power consumption as it passively reflects the incident signals without the need of any radio frequency chains. In addition, the radio signal reflected by the RIS is free from noise corruption or self-interference (SI) in an inherently full-duplex fashion [13]. Motivated by the aforementioned benefits of both the RIS and C-NOMA, the potential performance enhancement brought by effectively integrating RIS technology with C-NOMA-based cellular networks is investigated in this paper. This amalgamation between RIS and C-NOMA technologies can provide a promising paradigm for the upcoming 6G networks by providing additional paths that can jointly construct a stronger combined channel gain at the user of interest by leveraging the RIS technology and by improving the network connectivity by adopting the C-NOMA technique.

B. State-of-Art

The research on RIS-enabled NOMA-based cellular networks is gaining momentum to enhance and improve different performance metrics, such as power consumption [14]–[16], network spectral efficiency [17]–[19], network energy efficiency [20], user fairness [21], and physical layer security [22]. The authors in [14] evaluated the minimum power consumption in a two-UE NOMA network for three different multiple access schemes (frequency division multiple access, time division multiple access, and NOMA) to achieve the same required data rate threshold, and have proved that NOMA can achieve a superior performance compared to the counterpart OMA schemes in most of the system settings. The transmit beamforming at the BS, phase-shift matrix at the RIS and the channel gains ordering for a multi-UE NOMA cellular network were jointly optimized to minimize the total transmit power in [16]. With the goal of maximizing the sum-rate in a two-UE and multi-UE NOMA cellular

network, a joint optimization of the power allocation at the BS and the passive beamforming at the RIS were investigated in [17], [18], respectively. Aiming at improving the spectral efficiency of a multi-cell RIS-NOMA network, the problem of joint user association, sub-channel allocation, power control, and passive beamforming was formulated in [19]. By jointly optimizing the active beamforming at the BS and the passive beamforming at the RIS, an efficient algorithm was developed in [20] to maximize the network energy efficiency of a two-user RIS-NOMA network. A joint active beamforming at the BS and passive beamforming at the RIS was investigated in [21] to maximize the minimum achievable data rate, and accordingly, ensure user fairness.

Going deep into the investigation of RIS-NOMA cellular networks, the performance analysis using tools from stochastic geometry was considered in [23]–[26]. Specifically, the authors in [23] analyzed the network spectral efficiency when both the RIS technology and the coordinated multipoint transmission were jointly integrated in NOMA cellular networks. The network spectral efficiency, energy efficiency, and outage probability were derived in [24]. In [25], the RIS is used for assisting NOMA transmission when spatial division multiple access was applied by the BS to generate orthogonal beams for serving multiple two-UE NOMA clusters. Closed form expressions for the coverage probability and the ergodic rate were derived in an RIS assisted two-UE NOMA network in [26].

All the aforementioned research works [14]–[26] have only investigated the performance of integrating RIS with NOMA without considering the user-relaying cooperation, whilst there is a lack of investigations in the existing literature on the performance of C-NOMA when the RIS is considered in the network. Recently, the authors in [27] studied the performance of an RIS-assisted HD C-NOMA system by jointly optimizing the active beamforming at the BS, the user relaying power, and the phase shifts at the RIS. However, this work has not comprehensively analyzed the performance of RIS-aided HD C-NOMA compared to the FD C-NOMA, either with and without the RIS technology.

C. Contributions

Against the above background, and to the best of our knowledge, integrating RIS with C-NOMA in HD relaying mode has not been well studied in the literature and remains still unexplored. Moreover, this paper is one of the early attempts to explore the performance of FD C-NOMA systems with the assistance of RIS. These facts motivate this article to study the joint power allocation at the BS, transmit relaying power at the near UE, and passive beamforming at the RIS that minimize the total transmit power. Driven by the aforementioned observations, the main contributions of this paper can be summarized as follows.

- A downlink RIS-enabled HD/FD C-NOMA framework consisting of one BS, one near NOMA user, one far NOMA user, and one RIS is considered in this paper, where the near NOMA user can relay the message of the far NOMA user in either a HD or a FD relaying mode. For each relaying mode, this framework is formulated as an optimization problem with the objective of minimizing the total transmit power while guaranteeing the data rate QoS requirements for the users, the power budget at both BS and near NOMA user and the SIC constraint.
- Due to the high coupling between the power allocation coefficients at both the BS and near NOMA user from one side and the passive beamforming at the RIS from the other side, the formulated total transmit power minimization problem is neither linear nor convex, and hence, is difficult to be directly solved. In order to overcome this challenge, the alternating optimization approach is adopted, in which the original optimization problem is decomposed into two sub-problems, namely, a power allocation sub-problem and a phase-shift optimization sub-problem, which are solved in an alternating manner.
- For the power allocation sub-problem, and for given phase-shift matrices at the RIS, the feasibility conditions as relations between the QoS requirements, the power budget of the active nodes (BS and near NOMA user), and SIC constraints are derived. Then, the optimal solution of the power allocation sub-problem is determined in closed-form expressions, i.e., with a computational complexity of $\mathcal{O}(1)$.
- For the phase-shift optimization sub-problem, and for given values of the power allocation coefficients at the BS and fixed transmit relaying power at the near NOMA user, semi-definite relaxation (SDR) technique is applied to obtain a solution of the phase-shift matrix at the RIS.

Extensive simulations were carried out to evaluate the performance of the proposed RIS-enabled HD/FD C-NOMA cellular network. In order to validate the effectiveness of the proposed framework, the FD C-NOMA scheme without the assistance of the RIS was considered as a benchmark. The numerical results demonstrate the efficacy of the proposed framework compared to the FD C-NOMA without RIS scheme in terms of the total transmit power. In fact, the numerical results unveil that

- The RIS-enabled FD C-NOMA provides a significant gain in terms of the total transmit power compared to the RIS-enabled HD C-NOMA and the FD C-NOMA without RIS despite the existence of high residual SI at near NOMA user.
- The FD C-NOMA with the assistance of RIS has more resistance to the residual SI effect and can tolerate high SI values compared to the same system without RIS.
- RIS-enabled HD C-NOMA can beat the FD C-NOMA without RIS scheme despite the pre-log

TABLE I
TABLE OF NOTATIONS

System Parameters	
P_{BS}, P_n	Power budget of BS and UE _n , respectively.
R_n^{th} and R_f^{th}	Minimum required data rate for UE _n and UE _f , respectively.
$\beta^{\text{HD}}, \beta^{\text{FD}}$	Power fraction coefficients at UE _n in HD and FD relaying mode, respectively.
$\alpha_n^{\text{HD}}, \alpha_f^{\text{HD}}$	Power allocation coefficients at BS for UE _n and UE _f in the HD case, respectively.
$\alpha_n^{\text{FD}}, \alpha_f^{\text{FD}}$	Power allocation coefficients at BS for UE _n and UE _f in the FD case, respectively.
$\Theta_{(1)}^{\text{HD}}, \Theta_{(2)}^{\text{HD}}$	RIS phase-shift matrix in the first and second time slots, respectively, in the HD case.
Θ^{FD}	RIS phase-shift matrix in the FD case.
$\mathbf{h}_{\text{br}}, \mathbf{h}_{\text{rn}}, \mathbf{h}_{\text{rf}}, \mathbf{h}_{\text{nr}}$	Channel gains for BS-RIS, RIS-UE _n , RIS-UE _f , and UE _n -RIS links, respectively.
$h_{\text{bn}}, h_{\text{bf}}, h_{\text{nf}}$	Channel gains for BS-UE _n , BS-UE _f , UE _n -UE _f links, respectively.
$\hat{\mathbf{h}}_{\text{rf}}$	Channel gain for RIS-UE _f link in the second time-slot for the HD case.
η_x	Path-loss exponent for the communication link x .

penalty in the HD relaying mode. This performance gain depends on the number of RIS reflecting elements, the SI channel gain at the near NOMA user, and the required QoS at the NOMA users.

D. Paper Outline and Notations

The rest of the paper is organized as follows. Section II presents the system model of the proposed RIS-enabled C-NOMA system. Section III presents the signal-to-interference-plus-noise-ratio (SINR) and the rate analysis for both HD and FD relaying modes. Section IV and V present the formulated optimization problem and the solution approach for the RIS-enabled HD C-NOMA system and the RIS-enabled FD C-NOMA system, respectively. The simulation results and the conclusion are presented in Sections VI and VII, respectively.

The notations and symbols adopted throughout the paper are summarized in Table I. In addition, vectors and matrices are denoted by bold-face lower-case and upper-case letters, respectively. The distribution of a circularly symmetric complex Gaussian random vector with mean vector \mathbf{x} and covariance matrix Σ is denoted by $\mathcal{CN}(\mathbf{x}, \Sigma)$. For a complex-valued vector \mathbf{y} , $|\mathbf{y}|$ accounts for its Euclidean norm, $\arg(\mathbf{y})$ denotes a vector that contains the angles of the elements of \mathbf{y} , and $\text{diag}(\mathbf{y})$ denotes a diagonal matrix in which each element in the diagonal is the corresponding element in \mathbf{y} . For a square matrix \mathbf{S} , $\text{tr}(\mathbf{S})$ denotes its trace, while $\mathbf{S} \succeq \mathbf{0}$ means that \mathbf{S} is positive semi-definite. For any general matrix \mathbf{M} , \mathbf{M}^H and $\text{rank}(\mathbf{M})$ denote its conjugate transpose and rank, respectively. Moreover, $e^{(\cdot)}$ and $\exp(\cdot)$ denote the exponential function. Finally, $[\mathbf{h}]_n$ is the n th entry of \mathbf{h} .

II. SYSTEM MODEL

A. Network Model

We consider a downlink transmission in an RIS-enabled two-UE C-NOMA cellular system, which consists of one BS, one near UE denoted by UE_n, one far UE denoted by UE_f and one RIS equipped

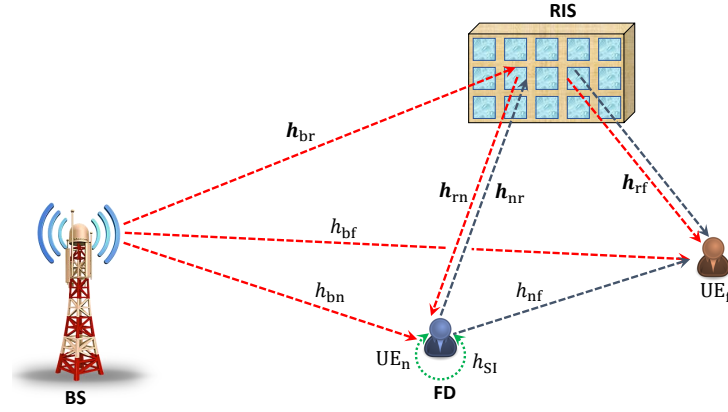


Fig. 1. RIS-enabled HD/FD C-NOMA cellular network.

with M reflecting elements as shown in Fig. 1. In the proposed model, UE_n has, on average, a better channel condition than UE_f , since UE_n is considered as the near UE and UE_f is deemed as the far UE. Therefore, in order to enhance the signal quality at the far NOMA UE, RIS is deployed near to UE_f . With the assistance of the RIS, the BS serves UE_n and UE_f simultaneously using NOMA, while UE_n relays the signal for UE_f either in a DF HD relaying mode or in a DF FD relaying mode. Let $h_{bn} \in \mathbb{C}$, $h_{bf} \in \mathbb{C}$, $\mathbf{h}_{br} \in \mathbb{C}^{M \times 1}$, $\mathbf{h}_{rn} \in \mathbb{C}^{M \times 1}$, $\mathbf{h}_{nr} \in \mathbb{C}^{M \times 1}$, $\mathbf{h}_{rf} \in \mathbb{C}^{M \times 1}$, $h_{nf} \in \mathbb{C}$, and h_{SI} be the channel coefficients of the communication links from BS \rightarrow UE_n , BS \rightarrow UE_f , BS \rightarrow RIS, RIS \rightarrow UE_n , $UE_n \rightarrow$ RIS, $UE_n \rightarrow$ UE_f , and of the SI link, respectively. Apart from h_{SI} , the small-scale fading and the large-scale fading are considered both for each communication link. Nevertheless, for all $y \in \{bn, bf, nf\}$ and $z \in \{rn, nr\}$, the small scale fading of h_y and \mathbf{h}_z are modeled as Rayleigh fading. Consequently, the corresponding channel coefficients can be expressed as

$$\begin{aligned} h_y &= g_y \sqrt{PL(d_y)}, \quad \forall y \in \{bn, bf, nf\}, \\ \mathbf{h}_z &= \mathbf{g}_z \sqrt{PL(d_z)}, \quad \forall z \in \{rn, nr\}, \end{aligned} \quad (1)$$

where $g_y \in \mathbb{C}$ and $\mathbf{g}_z \in \mathbb{C}^{M \times 1}$ are the small-scale Rayleigh fading with zero mean and unit variance, and $PL(d_y)$ and $PL(d_z)$ are the large-scale path-losses modelled, respectively, as $PL(d_y) = \rho_0 (\frac{d}{d_0})^{-\eta_y}$ and $PL(d_z) = \rho_0 (\frac{d}{d_0})^{-\eta_z}$, such that ρ_0 is the path-loss at a reference distance d_0 , η_y and η_z are the path-loss exponents, and d_y and d_z are the distance between the end-to-end nodes in the y th and z th links, respectively.

Considering the communication links between the BS and the RIS and between the RIS and UE_f , line-of-sight (LoS) components are assumed to exist [17]. Thus, these communication links experience

small-scale fading that are modelled as Rician fading. The corresponding channel coefficients for these communication links can be expressed as,

$$\mathbf{h}_x = \sqrt{PL(d_x)} \left(\sqrt{\frac{1}{1 + \kappa_x}} \mathbf{g}_x + \sqrt{\frac{\kappa_x}{1 + \kappa_x}} \hat{\mathbf{g}}_x \right), \quad \forall x \in \{\text{br, rf}\}, \quad (2)$$

where κ_x is the Rician factor, $\hat{\mathbf{g}}_x$ denotes the deterministic line-of-sight component and \mathbf{g}_x represents the non-line-of-sight component, which follows a Rayleigh distribution with mean zero and variance one. Due to the double fading effects of the BS-RIS-UE cascaded link, the cascaded communication link suffers from more severe path-loss than the direct communication link, i.e., the BS-UE link. Thus, it is assumed that the power of the reflected signals by the RIS two or more times can be ignored. The channel state information (CSI) of all the communication links is assumed to be perfectly known at the BS [14]–[21], [23]–[26].²

Since UE_n can adopt two different relaying modes, i.e., either HD or FD, two different transmission schemes, i.e., RIS-enabled HD C-NOMA and RIS-enabled FD C-NOMA, can be adopted, which are adequately defined in the next subsection.

B. Transmission Model

The transmission model for the two-UE C-NOMA consists of two phases (direct transmission phase and cooperative transmission phase) that are detailed as follows.

- **Direct transmission (DT) phase:** the BS applies superposition coding on the signals intended to UE_n and UE_f . Then, it transmits the superimposed signal to both of them. The transmitted signal by the BS will hit the RIS and will be then reflected back to UE_n and UE_f to improve their signals reception diversity. Following NOMA principle, UE_n first performs SIC to decode the intended signal for UE_f . Second, it cancels the decoded signal of the UE_f from its own reception. Afterwards, UE_n decodes its own signal from the resulting reception. Meanwhile, UE_f treats the signal of UE_n as a noise.
- **Cooperative transmission (CT) phase:** UE_n relays the decoded signal of UE_f through a D2D channel. Consequently, two signals will be received at the UE_f 's side. The first is resulting from the transmission of UE_n and the second signal comes from the reflection by the RIS. Finally, UE_f combines the received signals coming from the BS, RIS, and UE_n and then decodes its own signal.

²To characterize the theoretical performance gain and provide useful insights achieved by the amalgamation between RIS and C-NOMA, we assume that the CSI of all communication links is available at the BS. This CSI can be efficiently obtained by one of the channel estimation techniques for RIS-assisted wireless networks [28], [29].

For the case of HD relaying mode, the two transmission phases (DT and CT) occur in two consecutive time-slots. As shown in Fig. 1, the red lines represent the DT phase, which occurs in the first time-slot and the black lines show the CT phase, which occurs in the second time-slot. However, for the case of FD relaying mode, DT and CT occur in the same time-slot with the cost of inducing SI at UE_n (the green line in Fig. 1). After presenting the main operations of RIS-enabled HD C-NOMA and RIS-enabled FD C-NOMA, we direct our attention toward calculating the received SINR and the corresponding achievable data rates at UE_n and UE_f in the two different operation modes (FD and HD) as shown in the next section.

III. DOWNLINK SINRS MODEL AND ACHIEVABLE RATES ANALYSIS

In this section, we present the analysis of both the SINRs and the achievable rates for a C-NOMA-based cellular system assisted by RIS for both HD and FD relaying modes. For the two different relaying modes and at each channel use, the superimposed mixture of the signals intended to UE_n and UE_f at the BS are expressed, respectively, as

$$\begin{aligned}\mathcal{S}^{\text{HD}} &= \sqrt{\alpha_n^{\text{HD}} P_{\text{BS}}} \mathcal{S}_n + \sqrt{\alpha_f^{\text{HD}} P_{\text{BS}}} \mathcal{S}_f, \\ \mathcal{S}^{\text{FD}} &= \sqrt{\alpha_n^{\text{FD}} P_{\text{BS}}} \mathcal{S}_n + \sqrt{\alpha_f^{\text{FD}} P_{\text{BS}}} \mathcal{S}_f,\end{aligned}\quad (3)$$

where \mathcal{S}_n and \mathcal{S}_f represent the intended signals of UE_n and UE_f , respectively, such that $\mathbb{E}[|\mathcal{S}_n|^2] = 1$ and $\mathbb{E}[|\mathcal{S}_f|^2] = 1$, P_{BS} represents the power budget of the BS, and for $R \in \{\text{HD}, \text{FD}\}$, α_n^R and α_f^R represent the power control coefficients allocated by the BS to UE_n and UE_f in the relaying mode R , respectively. Therefore, for $R \in \{\text{HD}, \text{FD}\}$, the power allocated by the BS to UE_n and UE_f in the relaying mode R are $\alpha_n^R P_{\text{BS}}$ and $\alpha_f^R P_{\text{BS}}$, respectively.

A. RIS-enabled HD C-NOMA

For the case of RIS-enabled HD C-NOMA, the received signal at UE_n in the DT phase can be expressed as

$$\mathcal{Y}_n^{\text{HD}} = (h_{\text{bn}} + \mathbf{h}_{\text{rn}}^H \mathbf{\Theta}_{(1)}^{\text{HD}} \mathbf{h}_{\text{br}}) \mathcal{S}^{\text{HD}} + \mathcal{W}_n, \quad (4)$$

where $\mathcal{W}_n \sim (0, \sigma_n^2)$ is the additive white Gaussian noise (AWGN) with zero mean and variance σ_n^2 and $\mathbf{\Theta}_{(1)}^{\text{HD}} = \text{diag}\{e^{j\theta_1^{(1)}}, e^{j\theta_2^{(1)}}, \dots, e^{j\theta_M^{(1)}}\}$ is the phase-shift matrix of the RIS in the DT phase, where for all $m \in \llbracket 1, M \rrbracket$, $\theta_m^{(1)} \in [0, 2\pi]$ represents the phase shift of the m th reflecting element of the RIS in the first time slot. According to the NOMA principle, SIC is adopted at UE_n to decode the

message \mathcal{S}_f of UE_f . Consequently, the received SINR at UE_n to decode the message of UE_f can be expressed as

$$\text{SINR}_{n \rightarrow f}^{\text{HD}} = \frac{\alpha_f^{\text{HD}} P_{\text{BS}} |h_{\text{bn}} + \mathbf{h}_{\text{rn}}^H \mathbf{\Theta}_{(1)}^{\text{HD}} \mathbf{h}_{\text{br}}|^2}{\alpha_n^{\text{HD}} P_{\text{BS}} |h_{\text{bn}} + \mathbf{h}_{\text{rn}}^H \mathbf{\Theta}_{(1)}^{\text{HD}} \mathbf{h}_{\text{br}}|^2 + \sigma_n^2}. \quad (5)$$

Therefore, after cancelling UE_f 's message, the SINR at UE_n to decode its own message can be expressed as

$$\text{SINR}_{n \rightarrow n}^{\text{HD}} = \frac{\alpha_n^{\text{HD}} P_{\text{BS}} |h_{\text{bn}} + \mathbf{h}_{\text{rn}}^H \mathbf{\Theta}_{(1)}^{\text{HD}} \mathbf{h}_{\text{br}}|^2}{\sigma_n^2}. \quad (6)$$

Thus, the achievable data rate at UE_n to decode the message of UE_f and to decode its own message can be expressed, respectively, as

$$\mathcal{R}_{n \rightarrow f}^{\text{HD}} = \frac{1}{2} \log_2 (1 + \text{SINR}_{n \rightarrow f}^{\text{HD}}), \quad (7)$$

$$\mathcal{R}_{n \rightarrow n}^{\text{HD}} = \frac{1}{2} \log_2 (1 + \text{SINR}_{n \rightarrow n}^{\text{HD}}). \quad (8)$$

On the other hand, the received signal at UE_f in the DT phase is expressed as

$$\mathcal{Y}_f^{(1)} = (h_{\text{bf}} + \mathbf{h}_{\text{rf}}^H \mathbf{\Theta}_{(1)}^{\text{HD}} \mathbf{h}_{\text{br}}) \mathcal{S}^{\text{HD}} + \mathcal{W}_f^{(1)}, \quad (9)$$

where $\mathcal{W}_f^{(1)} \sim (0, \sigma_f^2)$ is the AWGN at UE_f in the first phase. Therefore, the received SINR at UE_f in the DT phase is given by

$$\text{SINR}_{(1)}^{\text{HD}} = \frac{\alpha_f^{\text{HD}} P_{\text{BS}} |h_{\text{bf}} + \mathbf{h}_{\text{rf}}^H \mathbf{\Theta}_{(1)}^{\text{HD}} \mathbf{h}_{\text{br}}|^2}{\alpha_n^{\text{HD}} P_{\text{BS}} |h_{\text{bf}} + \mathbf{h}_{\text{rf}}^H \mathbf{\Theta}_{(1)}^{\text{HD}} \mathbf{h}_{\text{br}}|^2 + \sigma_f^2}. \quad (10)$$

Meanwhile, in the CT phase, UE_n forwards the decoded message \mathcal{S}_f to UE_f . Consequently, the observation at UE_f in this phase resulting from the transmission of UE_n and the reflections by the RIS can be given by

$$\mathcal{Y}_f^{(2)} = \beta^{\text{HD}} P_n (h_{\text{nf}} + \hat{\mathbf{h}}_{\text{rf}}^H \mathbf{\Theta}_{(2)}^{\text{HD}} \mathbf{h}_{\text{nr}}) \mathcal{S}_f + \mathcal{W}_f^{(2)}, \quad (11)$$

where $\beta^{\text{HD}} \in [0, 1]$ is the fraction of the allocated power by UE_n , P_n is the power budget at UE_n , $\hat{\mathbf{h}}_{\text{rf}}^H$ is the channel gain between the RIS and UE_f in the CT phase and $\mathcal{W}_f^{(2)} \sim (0, \sigma_f^2)$ is the AWGN at UE_f in the CT phase. In addition, $\mathbf{\Theta}_{(2)}^{\text{HD}} = \text{diag}\{e^{j\theta_1^{(2)}}, e^{j\theta_2^{(2)}}, \dots, e^{j\theta_M^{(2)}}\}$ is the phase-shift matrix in the CT phase, where for all $m \in \llbracket 1, M \rrbracket$, $\theta_m^{(2)} \in [0, 2\pi]$ represents the phase shift of the m th reflecting element of the RIS in the second time-slot. Therefore, the received SINR at UE_f in the second phase can be expressed as

$$\text{SINR}_{(2)}^{\text{HD}} = \frac{\beta^{\text{HD}} P_n |h_{\text{nf}} + \hat{\mathbf{h}}_{\text{rf}}^H \mathbf{\Theta}_{(2)}^{\text{HD}} \mathbf{h}_{\text{nr}}|^2}{\sigma_f^2}. \quad (12)$$

Toward this end, the effective SINR at UE_f is the summation of the received SINRs in the DT and CT phases using maximum ratio combining (MRC) [30]. Based on this, the data rate of UE_f due to the MRC can be expressed as

$$\mathcal{R}_{\text{MRC}}^{\text{HD}} = \frac{1}{2} \log_2(1 + \text{SINR}_{(1)}^{\text{HD}} + \text{SINR}_{(2)}^{\text{HD}}). \quad (13)$$

However, the rate \mathcal{R}_{MRC} can be achievable if and only if UE_n has the ability to decode the message \mathcal{S}_f of UE_f . Thus, the data rate achieved at UE_f is bounded by the data rate of UE_n to decode the message of UE_f , i.e. $\mathcal{R}_{n \rightarrow f}$ [30]. Therefore, the achievable data rate of UE_f to decode its own message can be given as

$$\mathcal{R}_{f \rightarrow f}^{\text{HD}} = \min(\mathcal{R}_{n \rightarrow f}^{\text{HD}}, \mathcal{R}_{\text{MRC}}^{\text{HD}}). \quad (14)$$

B. RIS-enabled FD C-NOMA

For the case of RIS-enabled FD C-NOMA, both the DT and CT phases are executed simultaneously using the same radio channel. Due to this, UE_n suffers from a SI resulting from receiving data from the BS and transmitting data to the UE_f simultaneously within the same co-channel [31]. Hence, the received signal at UE_n is given by

$$\mathcal{Y}_n^{\text{FD}} = (h_{\text{bn}} + \mathbf{h}_{\text{rn}}^H \mathbf{\Theta}^{\text{FD}} \mathbf{h}_{\text{br}}) \mathcal{S}^{\text{FD}} + h_{\text{SI}} \tilde{\mathcal{S}}_f + \mathcal{W}_n, \quad (15)$$

where h_{SI} represents the SI channel coefficient at UE_n and $\tilde{\mathcal{S}}_f$ represents the transmit signal by UE_n to UE_f [32]. This transmission of $\tilde{\mathcal{S}}_f$ causes an interference at UE_n . In addition, $\mathbf{\Theta}^{\text{FD}} = \text{diag}\{e^{j\theta_1}, e^{j\theta_2}, \dots, e^{j\theta_M}\}$ is the phase-shift matrix, where for all $m \in \llbracket 1, M \rrbracket$, $\theta_m \in [0, 2\pi]$ represents the phase shift of the m th reflecting element of the RIS. Therefore, the achievable data rate of UE_n to decode the message of UE_f can be expressed as

$$\mathcal{R}_{n \rightarrow f}^{\text{FD}} = \log_2 \left[1 + \frac{\alpha_f^{\text{FD}} P_{\text{BS}} |h_{\text{bn}} + \mathbf{h}_{\text{rn}}^H \mathbf{\Theta}^{\text{FD}} \mathbf{h}_{\text{br}}|^2}{\alpha_n^{\text{FD}} P_{\text{BS}} |h_{\text{bn}} + \mathbf{h}_{\text{rn}}^H \mathbf{\Theta}^{\text{FD}} \mathbf{h}_{\text{br}}|^2 + \beta^{\text{FD}} P_n \gamma_{\text{SI}} + \sigma_n^2} \right], \quad (16)$$

where $\gamma_{\text{SI}} = |h_{\text{SI}}|^2$. Then, after the successive decoding and cancelling the signal of UE_f , UE_n decodes its own signal \mathcal{S}_n . Consequently, the achievable data rate of UE_n to decode its own signal can be given as

$$\mathcal{R}_{n \rightarrow n}^{\text{FD}} = \log_2 \left[1 + \frac{\alpha_n^{\text{FD}} P_{\text{BS}} |h_{\text{bn}} + \mathbf{h}_{\text{rn}}^H \mathbf{\Theta}^{\text{FD}} \mathbf{h}_{\text{br}}|^2}{\beta^{\text{FD}} P_n \gamma_{\text{SI}} + \sigma_n^2} \right]. \quad (17)$$

Afterwards, UE_n forwards the signal $\tilde{\mathcal{S}}_f$ to UE_f . Thus, the received signal at UE_f is given by

$$\mathcal{Y}_f^{\text{FD}} = (h_{\text{bf}} + \mathbf{h}_{\text{rf}}^H \mathbf{\Theta}^{\text{FD}} \mathbf{h}_{\text{br}}) \mathcal{S}^{\text{FD}} + \beta^{\text{FD}} P_n (h_{\text{nf}} + \mathbf{h}_{\text{rf}}^H \mathbf{\Theta}^{\text{FD}} \mathbf{h}_{\text{nr}}) \tilde{\mathcal{S}}_f + \mathcal{W}_f, \quad (18)$$

where the first term in (18) is due to the transmission of the BS, whereas the second term results from the transmission of the near user over the D2D communication link. Note that, in FD scenario, $\mathbf{h}_{\text{nr}} \triangleq \mathbf{h}_{\text{rn}}$. Moreover, UE_f receives its own message from the transmission of both BS and UE_n at approximately the same channel use [9], [33], [34]. Hence, according to [9], [33], [34], UE_f can successfully align, co-phase, and combine the signal \mathcal{S}_f transmitted from the BS and the signal $\tilde{\mathcal{S}}_f$ (which is in fact the signal \mathcal{S}_f of UE_f decoded by UE_n) forwarded from UE_n. Consequently, based on the above discussion and on the results of [9], [33], [34], the achievable data rate of UE_f can be expressed as

$$\mathcal{R}_{\text{MRC}}^{\text{FD}} = \log_2 \left[1 + \frac{\alpha_f^{\text{FD}} P_{\text{BS}} |h_{\text{bf}} + \mathbf{h}_{\text{rf}}^H \mathbf{\Theta}^{\text{FD}} \mathbf{h}_{\text{br}}|^2 + \beta^{\text{FD}} P_n |h_{\text{nf}} + \mathbf{h}_{\text{rf}}^H \mathbf{\Theta}^{\text{FD}} \mathbf{h}_{\text{nr}}|^2}{\alpha_n^{\text{FD}} P_{\text{BS}} |h_{\text{bf}} + \mathbf{h}_{\text{rf}}^H \mathbf{\Theta}^{\text{FD}} \mathbf{h}_{\text{br}}|^2 + \sigma_f^2} \right]. \quad (19)$$

Based on this analysis and according to what was explained in the HD case, the achievable data rate of UE_f to decode its own message can be given by

$$\mathcal{R}_{f \rightarrow f}^{\text{FD}} = \min(\mathcal{R}_{n \rightarrow f}^{\text{FD}}, \mathcal{R}_{\text{MRC}}^{\text{FD}}). \quad (20)$$

IV. RIS-ENABLED HD C-NOMA: PROBLEM FORMULATION AND SOLUTION APPROACH

A. Problem Formulation

With the quest of improving the performance of the proposed RIS-enabled HD C-NOMA, an optimization problem is formulated with the objective of minimizing the total transmit power by the BS and the near user. This proposed framework includes two different objectives: 1) Power control for both the BS and the near user and 2) Phase-shift for the RIS, i.e., finding the best RIS configuration in the first and second time slots to enhance the system performance. By optimizing the power allocation coefficients at the BS ($\alpha_n^{\text{HD}}, \alpha_f^{\text{HD}}$), the power fraction coefficient at the near user β^{HD} , and the phase-shift matrices for the RIS $\boldsymbol{\theta}_{(1)} = [\theta_1^{(1)}, \theta_2^{(1)}, \dots, \theta_M^{(1)}]$ and $\boldsymbol{\theta}_{(2)} = [\theta_1^{(2)}, \theta_2^{(2)}, \dots, \theta_M^{(2)}]$, the total transmit power minimization problem for the proposed RIS-enabled HD C-NOMA framework can be formulated as follows.

$$\text{OPT - HD : } \min_{\substack{\boldsymbol{\theta}_{(1)}, \boldsymbol{\theta}_{(2)}, \\ \alpha_n^{\text{HD}}, \alpha_f^{\text{HD}}, \beta^{\text{HD}}}} (\alpha_n^{\text{HD}} + \alpha_f^{\text{HD}}) P_{\text{BS}} + \beta^{\text{HD}} P_n, \quad (21a)$$

$$\text{s.t. } 0 \leq \alpha_n^{\text{HD}} \leq \alpha_f^{\text{HD}}, \quad (21b)$$

$$0 \leq \alpha_n^{\text{HD}} + \alpha_f^{\text{HD}} \leq 1, \quad (21c)$$

$$0 \leq \beta^{\text{HD}} \leq 1, \quad (21d)$$

$$\mathcal{R}_{n \rightarrow n}^{\text{HD}} \geq R_n^{\text{th}}, \quad (21e)$$

$$\mathcal{R}_{\text{MRC}}^{\text{HD}} \geq R_f^{\text{th}}, \quad (21\text{f})$$

$$\mathcal{R}_{\text{n} \rightarrow \text{f}}^{\text{HD}} \geq R_f^{\text{th}}, \quad (21\text{g})$$

$$0 \leq \theta_m^{(1)} \leq 2\pi, \quad \forall m \in \llbracket 1, M \rrbracket \quad (21\text{h})$$

$$0 \leq \theta_m^{(2)} \leq 2\pi, \quad \forall m \in \llbracket 1, M \rrbracket \quad (21\text{i})$$

where constraint (21b) represents the SIC constraint, and constraints (21c) and (21d) guarantee that the total transmit power by the BS and UE_n do not exceed their power budget, respectively. Constraints (21e)-(21g) represent the QoS constraints for UE_n and UE_f, where R_n^{th} and R_f^{th} represent the required QoS in terms of minimum data rate for UE_n and UE_f, respectively. It can be seen that it is challenging to solve OPT – HD directly due to the high coupling between the power allocation coefficients $(\alpha_n^{\text{HD}}, \alpha_f^{\text{HD}}, \beta^{\text{HD}})$ and the RIS phase-shift coefficients $(\boldsymbol{\theta}_{(1)}, \boldsymbol{\theta}_{(2)})$ as well as the non convexity of constraints (21e)-(21g). Therefore, problem OPT – HD is hard to be solved by common standard optimization techniques. Thus, it is necessary to transform problem OPT – HD into tractable sub-problems that can be solved alternatively. Toward this end, the alternating optimization approach is utilized to solve OPT – HD in an efficient manner.

Accordingly, unlike [27], which decomposes the main problem into the DT sub-problem and CT sub-problem, we divide problem OPT – HD into two sub-problems, i.e. power control optimization sub-problem and RIS passive beamforming (phase-shift coefficients) optimization sub-problem. This is because we seek for deriving optimal closed-form expressions for the power control coefficients $(\alpha_n^{\text{HD}}, \alpha_f^{\text{HD}}, \beta^{\text{HD}})$ as a function of the phase-shift coefficients $(\boldsymbol{\theta}_{(1)}, \boldsymbol{\theta}_{(2)})$. In particular, we start by optimizing the power allocation coefficients at the BS and the power fraction coefficient at the near UE given the phase-shift coefficients $\boldsymbol{\theta}_{(1)}$ and $\boldsymbol{\theta}_{(2)}$ at the RIS in the DT and CT phases. Then, once the optimal power allocation coefficients at the BS and at UE_n are obtained, we direct our attention to the optimal phase-shift coefficients of the RIS at the DT and CT phases. Based on the above discussion, the power control optimization problem can be written as

$$\text{PC} - \text{HD} : \min_{\alpha_n^{\text{HD}}, \alpha_f^{\text{HD}}, \beta^{\text{HD}}} (\alpha_n^{\text{HD}} + \alpha_f^{\text{HD}}) P_{\text{BS}} + \beta^{\text{HD}} P_n, \quad (22\text{a})$$

$$\text{s.t. (21b) – (21g)}, \quad (22\text{b})$$

whereas the passive beamforming optimization problem can be presented as

$$\text{PS} - \text{HD} : \text{Find } \boldsymbol{\theta}_{(1)}, \boldsymbol{\theta}_{(2)} \quad (23\text{a})$$

$$\text{s.t. (21e) – (21i)} \quad (23\text{b})$$

B. RIS-enabled HD C-NOMA: Power Control Optimization

In this part, we assume that the phase shift matrices $\Theta_{(1)}^{\text{HD}}$ and $\Theta_{(2)}^{\text{HD}}$ are fixed. Based on this, we denote by

$$\gamma_{\text{bn}} \triangleq \frac{P_{\text{BS}} |h_{\text{bn}} + \mathbf{h}_{\text{rn}}^H \Theta_{(1)}^{\text{HD}} \mathbf{h}_{\text{br}}|^2}{\sigma_{\text{n}}^2}, \quad \gamma_{\text{bf}} \triangleq \frac{P_{\text{BS}} |h_{\text{bf}} + \mathbf{h}_{\text{rf}}^H \Theta_{(1)}^{\text{HD}} \mathbf{h}_{\text{br}}|^2}{\sigma_{\text{f}}^2}, \quad \text{and} \quad \gamma_{\text{d}} \triangleq \frac{P_{\text{n}} |h_{\text{nf}} + \hat{\mathbf{h}}_{\text{rf}}^H \Theta_{(2)}^{\text{HD}} \mathbf{h}_{\text{nr}}|^2}{\sigma_{\text{f}}^2}. \quad (24)$$

Before deriving the optimal power control of problem PC – HD, one needs to specify its feasibility conditions. The feasibility conditions of problem PC – HD define the conditions under which at least one feasible solution for this problem does exist. In addition, a feasible solution for problem PC – HD defines a solution that satisfies the constraint of this problem. In this context, the feasibility conditions of problem PC – HD are presented in the following theorem.

Theorem 1. *Problem PC – HD is feasible if and only if the following conditions hold.*

$$\text{Condition 1: } \alpha_{\text{min}}^{\text{HD}} \leq \alpha_{\text{max}}^{\text{HD}}, \quad (25\text{a})$$

$$\text{Condition 2: } \beta_{\text{min}}^{\text{HD}} \leq \beta_{\text{max}}^{\text{HD}}, \quad (25\text{b})$$

where $\alpha_{\text{min}}^{\text{HD}}$, $\alpha_{\text{max}}^{\text{HD}}$, $\beta_{\text{min}}^{\text{HD}}$ and $\beta_{\text{max}}^{\text{HD}}$ are expressed, respectively, as

$$\begin{aligned} \alpha_{\text{min}}^{\text{HD}} &= \frac{t_{\text{n}}^{\text{HD}}}{\gamma_{\text{bn}}}, & \alpha_{\text{max}}^{\text{HD}} &= \min \left(0, \frac{\gamma_{\text{bn}} - t_{\text{f}}^{\text{HD}}}{\gamma_{\text{bn}} (t_{\text{f}}^{\text{HD}} + 1)} \right), \\ \beta_{\text{min}}^{\text{HD}} &= \max \left(0, \frac{1}{\gamma_{\text{d}}} \left(t_{\text{f}}^{\text{HD}} - \frac{\gamma_{\text{bn}} - t_{\text{n}}^{\text{HD}}}{t_{\text{n}}^{\text{HD}} + \frac{\gamma_{\text{bn}}}{\gamma_{\text{bf}}}} \right) \right), & \beta_{\text{max}}^{\text{HD}} &= 1, \end{aligned} \quad (26)$$

such that $t_{\text{n}}^{\text{HD}} = 2^{2R_{\text{n}}^{\text{th}}} - 1$ and $t_{\text{f}}^{\text{HD}} = 2^{2R_{\text{f}}^{\text{th}}} - 1$.

Proof. See Appendix A. □

Afterwards, assuming that problem PC – HD is feasible, its optimal solution is given in the following theorem.

Theorem 2. *Assuming that problem PC – HD is feasible, i.e., conditions (25a) and (25b) hold, its optimal solution is expressed as follows. Let \mathbf{p}_1^{HD} and \mathbf{p}_2^{HD} denote the power control scheme expressed, respectively, as*

$$\mathbf{p}_1^{\text{HD}} = (\alpha_{\text{n},1}^{\text{HD}}, \alpha_{\text{f},1}^{\text{HD}}, \beta_1^{\text{HD}}) = \left(\alpha_{\text{min}}^{\text{HD}}, \max \left(\alpha_{\text{min}}^{\text{HD}}, \alpha_{\text{min}}^{\text{HD}} t_{\text{f}}^{\text{HD}} + \frac{t_{\text{f}}^{\text{HD}}}{\gamma_{\text{n}}} \right), \frac{1}{\gamma_{\text{d}}} \left(t_{\text{f}}^{\text{HD}} - \frac{\alpha_{\text{f},1}^{\text{HD}} \gamma_{\text{f}}}{\alpha_{\text{n},1}^{\text{HD}} \gamma_{\text{f}} + 1} \right) \right), \quad (27\text{a})$$

$$\mathbf{p}_2^{\text{HD}} = (\alpha_{\text{n},2}^{\text{HD}}, \alpha_{\text{f},2}^{\text{HD}}, \beta_2^{\text{HD}}) = \left(\alpha_{\text{min}}^{\text{HD}}, \frac{(\alpha_{\text{min}}^{\text{HD}} \gamma_{\text{bn}} + 1) t_{\text{f}}^{\text{HD}}}{\gamma_{\text{bn}}}, 0 \right). \quad (27\text{b})$$

Then, the optimal power control scheme is expressed as

$$\mathbf{p}^{\text{HD}*} = (\alpha_n^{\text{HD}*}, \alpha_f^{\text{HD}*}, \beta^{\text{HD}*}) = \underset{\mathbf{p}^{\text{HD}} \in \{\mathbf{p}_1^{\text{HD}}, \mathbf{p}_2^{\text{HD}}\}}{\operatorname{argmin}} f(\mathbf{p}^{\text{HD}}), \quad (28)$$

where the function f is the objective function of problem PC – HD, i.e.,

$$f(\mathbf{p}^{\text{HD}}) = f(\alpha_n^{\text{HD}}, \alpha_f^{\text{HD}}, \beta^{\text{HD}}) = (\alpha_n^{\text{HD}} + \alpha_f^{\text{HD}})P_{\text{BS}} + \beta^{\text{HD}}P_n. \quad (29)$$

Proof. See Appendix B. □

C. RIS-enabled HD C-NOMA: Phase-Shift Coefficients Optimization

In this subsection, the phase-shift coefficients in both DT and CT phases are optimized with given values of $(\alpha_n^{\text{HD}}, \alpha_f^{\text{HD}}, \beta^{\text{HD}})$. One can see that PS – HD is a feasibility check problem (finding the phase-shift coefficient for each element such that the QoS constraints are satisfied). Note that, the RIS provides additional paths to construct a stronger combined channel gain at the intended receiver. Therefore, the best channel gain in the second time-slot can be achieved when the reflected signals from the RIS can be constructively added at UE_f and be co-phased with the direct D2D link from UE_n to UE_f . As a result, optimal phase-shift coefficients in CT phase can be obtained as follows [23], [35].

$$\theta_m^{(2)} = \arg(h_{\text{nf}}) - \arg([\mathbf{h}_{\text{nr}}]_m [\hat{\mathbf{h}}_{\text{rf}}]_m). \quad (30)$$

Consequently, $\text{SINR}_{(2)}^{\text{HD}}$ can be expressed as

$$\text{SINR}_{(2)}^{\text{HD}} = \frac{\beta^{\text{HD}} P_n (|h_{\text{nf}}| + \sum_{m=1}^M |[\hat{\mathbf{h}}_{\text{rf}}]_m [\mathbf{h}_{\text{nr}}]_m|)^2}{\sigma_f^2}. \quad (31)$$

After obtaining the optimal value for $\theta_{(2)}^{\text{HD}}$, the SDR technique is applied for obtaining $\theta_{(1)}^{\text{HD}}$. Let us start by defining $\mathbf{v} = [v_1, \dots, v_M]^H$, where for all $m \in \llbracket 1, M \rrbracket$, $v_m = e^{j\theta_m}$. Then, the constraints in (21h) are equivalent to the unit-modulus constraints, i.e., $|v_m|^2 = 1$ for all $m \in \llbracket 1, M \rrbracket$. By applying the change of variables $\mathbf{h}_{\text{rn}}^H \Theta_{(1)}^{\text{HD}} \mathbf{h}_{\text{br}} = \mathbf{v}^H \Phi$, where $\Phi = \text{diag}(\mathbf{h}_{\text{rn}}^H) \mathbf{h}_{\text{br}} \in \mathbb{C}^{M \times 1}$ and $\mathbf{h}_{\text{rf}}^H \Theta \mathbf{h}_{\text{br}} = \mathbf{v}^H \Psi$, where $\Psi = \text{diag}(\mathbf{h}_{\text{rf}}^H) \mathbf{h}_{\text{br}} \in \mathbb{C}^{M \times 1}$, we have

$$|h_{\text{bn}} + \mathbf{h}_{\text{rn}}^H \Theta \mathbf{h}_{\text{br}}|^2 = |h_{\text{bn}} + \mathbf{v}^H \Phi|^2 \quad \text{and} \quad |h_{\text{bf}} + \mathbf{h}_{\text{rf}}^H \Theta \mathbf{h}_{\text{br}}|^2 = |h_{\text{bf}} + \mathbf{v}^H \Psi|^2. \quad (32)$$

By introducing an auxiliary variable t , then an equivalent representation of the achievable data rates

$\mathcal{R}_{n \rightarrow n}^{\text{HD}}$, $\mathcal{R}_{\text{MRC}}^{\text{HD}}$, and $\mathcal{R}_{n \rightarrow f}^{\text{HD}}$ can be expressed as follows

$$\mathcal{R}_{n \rightarrow n}^{\text{HD}} = \log \left(1 + \frac{\alpha_n^{\text{HD}} P_{\text{BS}} (\bar{\mathbf{v}}^H \mathbf{Q}_{\text{bn}} \bar{\mathbf{v}} + |h_{\text{bn}}|^2)}{\sigma_n^2} \right), \quad (33)$$

$$\mathcal{R}_{\text{MRC}}^{\text{HD}} = \log \left(1 + \frac{\alpha_f^{\text{HD}} P_{\text{BS}} (\bar{\mathbf{v}}^H \mathbf{Q}_{\text{bf}} \bar{\mathbf{v}} + |h_{\text{bf}}|^2)}{\alpha_n^{\text{HD}} P_{\text{BS}} (\bar{\mathbf{v}}^H \mathbf{Q}_{\text{bf}} \bar{\mathbf{v}} + |h_{\text{bf}}|^2) + \sigma_f^2} + \text{SINR}_{(2)}^{\text{HD}} \right), \quad (34)$$

$$\mathcal{R}_{n \rightarrow f}^{\text{HD}} = \log \left(1 + \frac{\alpha_f^{\text{HD}} P_{\text{BS}}(\bar{\mathbf{v}}^H \mathbf{Q}_{\text{bn}} \bar{\mathbf{v}} + |h_{\text{bn}}|^2)}{\alpha_n^{\text{HD}} P_{\text{BS}}(\bar{\mathbf{v}}^H \mathbf{Q}_{\text{bn}} \bar{\mathbf{v}} + |h_{\text{bn}}|^2) + \sigma_n^2} \right), \quad (35)$$

where

$$\mathbf{Q}_{\text{bn}} = \begin{bmatrix} \Phi \Phi^H & \Phi h_{\text{bn}}^H \\ h_{\text{bn}} \Phi^H & 0 \end{bmatrix}, \quad \mathbf{Q}_{\text{bf}} = \begin{bmatrix} \Psi \Psi^H & \Psi h_{\text{bf}}^H \\ h_{\text{bf}} \Psi^H & 0 \end{bmatrix} \quad \text{and} \quad \bar{\mathbf{v}} = \begin{bmatrix} \mathbf{v} \\ t \end{bmatrix}. \quad (36)$$

Note that $\bar{\mathbf{v}}^H \mathbf{Q}_z \bar{\mathbf{v}} = \text{tr}(\mathbf{Q}_z \bar{\mathbf{v}} \bar{\mathbf{v}}^H)$ for all $z \in \{\text{bn}, \text{bf}\}$. In addition, define $\mathbf{V} = \bar{\mathbf{v}} \bar{\mathbf{v}}^H$, which needs to satisfy $\text{rank}(\mathbf{V}) = 1$ and $\mathbf{V} \succeq \mathbf{0}$. This rank-one constraint ($\text{rank}(\mathbf{V}) = 1$) is non-convex [36]. Consequently, by dropping this constraint, PS – HD can be rewritten as

$$\mathcal{P} : \text{Find } \boldsymbol{\theta}_{(1)}^{\text{HD}} \quad (37\text{a})$$

$$\text{s.t. } \alpha_n^{\text{HD}} P_{\text{BS}}(\text{tr}(\mathbf{Q}_{\text{bn}} \mathbf{V}) + |h_{\text{bn}}|^2) \geq t_n^{\text{HD}} \sigma_n^2, \quad (37\text{b})$$

$$\alpha_f^{\text{HD}} P_{\text{BS}}(\text{tr}(\mathbf{Q}_{\text{bf}} \mathbf{V}) + |h_{\text{bf}}|^2) \geq (t_f^{\text{HD}} - \text{SINR}_{(2)}^{\text{HD}})(\alpha_n^{\text{HD}} P_{\text{BS}}(\text{tr}(\mathbf{Q}_{\text{bf}} \mathbf{V}) + |h_{\text{bf}}|^2) + \sigma_f^2), \quad (37\text{c})$$

$$\alpha_f^{\text{HD}} P_{\text{BS}}(\text{tr}(\mathbf{Q}_{\text{bn}} \mathbf{V}) + |h_{\text{bn}}|^2) \geq t_f^{\text{HD}} (\alpha_n^{\text{HD}} P_{\text{BS}}(\text{tr}(\mathbf{Q}_{\text{bn}} \mathbf{V}) + |h_{\text{bn}}|^2) + \sigma_n^2), \quad (37\text{d})$$

$$\mathbf{V} \succeq \mathbf{0}, \quad (37\text{e})$$

$$[\mathbf{V}]_{m,m} = 1, \quad \forall m \in [1, M+1]. \quad (37\text{f})$$

It is not difficult to observe that problem \mathcal{P} is a semi-definite programming (SDP) problem and hence it can be optimally solved by existing convex optimization solvers such as CVX [36]. In general, the optimal \mathbf{V} obtained by solving problem \mathcal{P} does not satisfy the rank-one constraint. This implies that the optimal solution of problem \mathcal{P} only serves as an upper bound for PS – HD. Consequently, additional steps are required to construct a rank-one solution, which can be achieved by applying the Gaussian randomization scheme to obtain a rank-one solution. This can be described as follows. First, we obtain the eigenvalue decomposition of \mathbf{V} as $\mathbf{V} = \mathbf{U} \boldsymbol{\Sigma} \mathbf{U}^H$, where $\mathbf{U} = [u_1, u_2, \dots, u_{M+1}]$ is a unitary matrix and $\boldsymbol{\Sigma} = \text{diag}(\lambda_1, \lambda_2, \dots, \lambda_{M+1})$ is a diagonal matrix, respectively. After that, a random vector is generated as $\bar{\mathbf{v}} = \mathbf{U} \boldsymbol{\Sigma}^{1/2} \mathbf{r}$, where \mathbf{r} is a random vector that follows a circularly symmetric complex Gaussian (CSCG) distribution with a zero mean and a co-variance matrix equal to the identity matrix of order $M+1$, denoted by \mathbf{I}_{M+1} , i.e., $\mathbf{r} \sim \mathcal{CN}(\mathbf{0}, \mathbf{I}_{M+1})$. Furthermore, we generate the scalar $v = \exp \left[j \arg \left(\frac{[\bar{\mathbf{v}}]_{1:M}}{[\bar{\mathbf{v}}]_{M+1}} \right) \right]$, where $[\mathbf{x}]_{1:M}$ denotes a vector having the first M elements in \mathbf{x} . It is important to mention that the SDR approach followed by a large number of Gauss randomization can guarantee a minimum accuracy of $\pi/4$ of the optimal objective value [36]. Finally, the steps of the proposed optimization scheme for RIS-enabled HD C-NOMA are presented in details in **Algorithm 1**. The convergence of the alternating optimization technique is guaranteed and the proof details can be found in [37].

Algorithm 1: Alternating Optimization Algorithm for RIS-enabled HD C-NOMA

Input: $P_{\text{BS}}, P_{\text{n}}, \mathbf{Q}_{\text{bn}}, \mathbf{Q}_{\text{bf}}, \sigma_{\text{n}}^2, \sigma_{\text{f}}^2$ and $\text{SINR}_{(2)}^{\text{HD}}$

- 1 Initialize the phase-shift $\theta_{(1)}^{\text{HD},0}$ and set the iteration number $l = 1$
 - 2 **repeat**
 - 3 Using the closed-form expressions in *Theorem 2* to find the optimal power allocation coefficients at the BS $(\alpha_{\text{n}}^{\text{HD},l}, \alpha_{\text{f}}^{\text{HD},l})$ and the optimal power fraction coefficient at UE_n, i.e. $\beta^{\text{HD},l}$ for given $\theta_{(1)}^{\text{HD},l}$
 - 4 Solve problem \mathcal{P} for given power allocation coefficients $(\alpha_{\text{n}}^{\text{HD},l}, \alpha_{\text{f}}^{\text{HD},l}, \beta^{\text{HD},l})$
 - 5 Obtain an approximate solution for the phase-shift using eigenvalue decomposition and Gauss randomization approach. Then, denote the solution as $\theta_{(1)}^{\text{HD},l}$
 - 6 Update $l = l + 1$
 - 7 **Until** The decrease of the objective value in (21) is below a threshold $\epsilon > 0$ or the maximum number of iterations L is reached
-

V. RIS-ENABLED FD C-NOMA: PROBLEM FORMULATION AND SOLUTION APPROACH

A. Problem Formulation

In this subsection, we investigate the power minimization problem for RIS-enabled FD C-NOMA systems. In the FD C-NOMA, UE_n decodes the message of UE_f and then forwards it to UE_f through the D2D direct link with the aid of the RIS in the same time-slot. As a result, in contrast to the HD scenario that requires two time-slot and adjusts the RIS's configuration in each one of them, only one RIS's configuration is required in the FD case. By optimizing the power allocation coefficients at the BS $(\alpha_{\text{n}}^{\text{FD}}, \alpha_{\text{f}}^{\text{FD}})$, the power fraction coefficient at UE_n, β^{FD} , and the phase-shift coefficients for the RIS $\theta^{\text{FD}} = [\theta_1, \theta_2, \dots, \theta_M]$, the total transmit power minimization problem for the proposed RIS-enabled FD C-NOMA framework can be formulated as follows.

$$\text{OPT - FD} : \min_{\substack{\theta_{\text{n}}^{\text{FD}}, \alpha_{\text{n}}^{\text{FD}}, \\ \alpha_{\text{f}}^{\text{FD}}, \beta^{\text{FD}}}} (\alpha_{\text{n}}^{\text{FD}} + \alpha_{\text{f}}^{\text{FD}})P_{\text{BS}} + \beta^{\text{FD}}P_{\text{n}}, \quad (38\text{a})$$

$$\text{s.t. } 0 \leq \alpha_{\text{n}}^{\text{FD}} \leq \alpha_{\text{f}}^{\text{FD}}, \quad (38\text{b})$$

$$0 \leq \alpha_{\text{n}}^{\text{FD}} + \alpha_{\text{f}}^{\text{FD}} \leq 1, \quad (38\text{c})$$

$$0 \leq \beta^{\text{FD}} \leq 1, \quad (38\text{d})$$

$$\mathcal{R}_{\text{n} \rightarrow \text{n}}^{\text{FD}} \geq R_{\text{n}}^{\text{th}}, \quad (38\text{e})$$

$$\mathcal{R}_{\text{MRC}}^{\text{FD}} \geq R_{\text{f}}^{\text{th}}, \quad (38\text{f})$$

$$\mathcal{R}_{\text{n} \rightarrow \text{f}}^{\text{FD}} \geq R_{\text{f}}^{\text{th}}, \quad (38\text{g})$$

$$0 \leq \theta_m \leq 2\pi, \quad \forall m \in \llbracket 1, M \rrbracket \quad (38h)$$

Similar to OPT – HD, OPT – FD is hard to be solved by common standard optimization techniques. Therefore, we resort to the alternating optimization technique similar to the RIS-enabled HD C-NOMA case in solving problem OPT – FD. Consequently, the power control optimization problem with a fixed $\boldsymbol{\theta}^{\text{FD}}$ can be written as

$$\text{PC – FD : } \min_{\alpha_n^{\text{FD}}, \alpha_f^{\text{FD}}, \beta^{\text{FD}}} (\alpha_n^{\text{FD}} + \alpha_f^{\text{FD}}) P_{\text{BS}} + \beta^{\text{FD}} P_n, \quad (39a)$$

$$\text{s.t. (38b) – (38g),} \quad (39b)$$

whereas the passive beamforming optimization problem with given power allocation coefficients, i.e., α_n^{FD} , α_f^{FD} and β^{FD} can be presented as

$$\text{PS – FD : Find } \boldsymbol{\theta}^{\text{FD}}, \quad (40a)$$

$$\text{s.t. (38e) – (38h).} \quad (40b)$$

B. RIS-enabled FD C-NOMA: Power Allocation Optimization

In this part, we start by determining the feasibility conditions of problem PC – FD. Assuming that the phase shift matrix $\boldsymbol{\Theta}^{\text{FD}}$ is fixed, we denote by $\gamma_{\text{SI}} \triangleq \frac{P_n \gamma_{\text{SI}}}{\sigma_n^2}$ and by

$$\gamma_{\text{bn}} \triangleq \frac{P_{\text{BS}} |h_{\text{bn}} + \mathbf{h}_{\text{rn}}^H \boldsymbol{\Theta}^{\text{FD}} \mathbf{h}_{\text{br}}|^2}{\sigma_n^2}, \quad \gamma_{\text{bf}} \triangleq \frac{P_{\text{BS}} |h_{\text{bf}} + \mathbf{h}_{\text{rf}}^H \boldsymbol{\Theta}^{\text{FD}} \mathbf{h}_{\text{br}}|^2}{\sigma_f^2}, \quad \text{and} \quad \gamma_{\text{d}} \triangleq \frac{P_n |h_{\text{nf}} + \mathbf{h}_{\text{rf}}^H \boldsymbol{\Theta}^{\text{FD}} \mathbf{h}_{\text{nr}}|^2}{\sigma_f^2}, \quad (41)$$

Based on this, the feasibility conditions of problem PC – FD are presented in the following theorem.

Theorem 3. *Problem PC – FD is feasible if and only if the following conditions hold.*

$$\text{Condition 1: } \beta_{\text{min}}^{\text{FD}} \leq \beta_{\text{max}}^{\text{FD}}, \quad (42a)$$

$$\text{Condition 2: } \frac{\gamma_{\text{SI}} t_n^{\text{FD}}}{\gamma_{\text{bn}}} \beta_{\text{min}}^{\text{FD}} + \frac{t_n^{\text{FD}}}{\gamma_{\text{bn}}} \leq \frac{1}{2}, \quad (42b)$$

where $\beta_{\text{min}}^{\text{FD}}$ and $\beta_{\text{max}}^{\text{FD}}$ are expressed, respectively, as

$$\beta_{\text{min}}^{\text{HD}} = \max \left(0, \frac{\gamma_{\text{bf}} - t_f^{\text{FD}} - \frac{\gamma_{\text{bf}}(1+t_f^{\text{FD}})t_n^{\text{FD}}}{\gamma_n}}{c_1 - c_2} \right) \quad \text{and} \quad \beta_{\text{max}}^{\text{HD}} = \min \left(1, \frac{\gamma_n - t_f^{\text{FD}} - t_n^{\text{FD}}(1+t_f^{\text{FD}})}{\gamma_{\text{SI}} t_n^{\text{FD}}(1+t_f^{\text{FD}}) + t_f^{\text{FD}}} \right), \quad (43)$$

if $c_1 < c_2$ and

$$\beta_{\text{min}}^{\text{HD}} = 0, \quad \text{and} \quad \beta_{\text{max}}^{\text{HD}} = \min \left(1, \frac{\gamma_n - t_f^{\text{FD}} - t_n^{\text{FD}}(1+t_f^{\text{FD}})}{\gamma_{\text{SI}} t_n^{\text{FD}}(1+t_f^{\text{FD}}) + t_f^{\text{FD}}}, \frac{\gamma_{\text{bf}} - t_f^{\text{FD}} - \frac{\gamma_{\text{bf}}(1+t_f^{\text{FD}})t_n^{\text{FD}}}{\gamma_n}}{c_1 - c_2} \right), \quad (44)$$

if $c_1 > c_2$, such that $c_1 = \frac{\gamma_{bf}}{\gamma_n} (1 + t_f^{\text{FD}}) t_n^{\text{FD}} \gamma_{\text{SI}}$, $c_2 = \gamma_d$, $t_n^{\text{FD}} = 2^{R_n^{\text{th}}} - 1$ and $t_f^{\text{FD}} = 2^{R_n^{\text{th}}} - 1$.

Proof. See Appendix C. □

Before continuing with the derivation of the optimal power control, let us define the following quantities. Let β_c^{FD} , α_c^{FD} , $\alpha_{\min}^{\text{FD}}$ and $\alpha_{\max}^{\text{FD}}$ be defined, respectively, as

$$\begin{aligned} \beta_c^{\text{FD}} &\triangleq \frac{t_f^{\text{FD}} \left(1 - \frac{\gamma_{bn}}{\gamma_{bf}}\right)}{\frac{\gamma_{bn}}{\gamma_{bf}} \gamma_{\text{SI}} t_f^{\text{FD}} + \gamma_d}, & \alpha_c^{\text{FD}} &\triangleq \frac{\gamma_{\text{SI}} t_n^{\text{FD}}}{\gamma_{bn}} \beta_c^{\text{FD}} + \frac{t_n^{\text{FD}}}{\gamma_{bn}}, \\ \alpha_{\min}^{\text{FD}} &\triangleq \frac{\gamma_{\text{SI}} t_n^{\text{FD}}}{\gamma_{bn}} \beta_{\min}^{\text{FD}} + \frac{t_n^{\text{FD}}}{\gamma_{bn}}, & \alpha_{\max}^{\text{FD}} &\triangleq \frac{\gamma_{\text{SI}} t_n^{\text{FD}}}{\gamma_{bn}} \beta_{\max}^{\text{FD}} + \frac{t_n^{\text{FD}}}{\gamma_{bn}}, \end{aligned} \quad (45)$$

and let α_0^{FD} and β_0^{FD} be the quantities defined, respectively, as

$$(\alpha_0^{\text{FD}}, \beta_0^{\text{FD}}) = \begin{cases} (\alpha_{\min}^{\text{FD}}, \beta_{\min}^{\text{FD}}), & \text{if } \beta_c^{\text{FD}} < \beta_{\min}^{\text{FD}}, \\ (\alpha_c^{\text{FD}}, \beta_c^{\text{FD}}), & \text{if } \beta_c^{\text{FD}} \in [\beta_{\min}^{\text{FD}}, \beta_{\max}^{\text{FD}}], \\ (\alpha_{\max}^{\text{FD}}, \beta_{\max}^{\text{FD}}), & \text{otherwise.} \end{cases} \quad (46)$$

Based on the above definitions, let α_n^{FD} and β^{FD} be the vectors defined as

$$\begin{cases} \alpha_n^{\text{FD}} \triangleq (\alpha_{\min}^{\text{FD}}, \alpha_0^{\text{FD}}, \alpha_{\max}^{\text{FD}}) & \text{and } \beta^{\text{FD}} \triangleq (\beta_{\min}^{\text{FD}}, \beta_0^{\text{FD}}, \beta_{\max}^{\text{FD}}), & \text{if } \alpha_0^{\text{FD}} \leq \frac{1}{2} & \text{and } \alpha_{\max}^{\text{FD}} \leq \frac{1}{2}, \\ \alpha_n^{\text{FD}} \triangleq (\alpha_{\min}^{\text{FD}}, \alpha_0^{\text{FD}}) & \text{and } \beta^{\text{FD}} \triangleq (\beta_{\min}^{\text{FD}}, \beta_0^{\text{FD}}), & \text{if } \alpha_0^{\text{FD}} \leq \frac{1}{2} & \text{and } \alpha_{\max}^{\text{FD}} \geq \frac{1}{2}, \\ \alpha_n^{\text{FD}} \triangleq (\alpha_{\min}^{\text{FD}}, \alpha_{\max}^{\text{FD}}) & \text{and } \beta^{\text{FD}} \triangleq (\beta_{\min}^{\text{FD}}, \beta_{\max}^{\text{FD}}), & \text{if } \alpha_0^{\text{FD}} \geq \frac{1}{2} & \text{and } \alpha_{\max}^{\text{FD}} \leq \frac{1}{2}, \\ \alpha_n^{\text{FD}} \triangleq \alpha_{\min}^{\text{FD}} & \text{and } \beta^{\text{FD}} \triangleq \beta_{\min}^{\text{FD}}, & \text{if } \alpha_0^{\text{FD}} \geq \frac{1}{2} & \text{and } \alpha_{\max}^{\text{FD}} \geq \frac{1}{2}. \end{cases} \quad (47)$$

Let $L \in \{1, 2, 3\}$ be the number of elements of α_n^{FD} (or β^{FD} equivalently). Then, let \mathbf{x}_1^{FD} and \mathbf{x}_2^{FD} be the $2 \times L$ vectors defined, respectively, as $\mathbf{x}_1^{\text{FD}} \triangleq t_f^{\text{FD}} \alpha_n^{\text{FD}} + \frac{\gamma_{\text{SI}} t_f^{\text{FD}}}{\gamma_{bn}} \beta^{\text{FD}} + \frac{t_f^{\text{FD}}}{\gamma_{bn}}$ and $\mathbf{x}_2^{\text{FD}} \triangleq t_f^{\text{FD}} \alpha_n^{\text{FD}} - \frac{\gamma_d}{\gamma_{bf}} \beta^{\text{FD}} + \frac{t_f^{\text{FD}}}{\gamma_{bf}}$. Finally, let α_f^{FD} be the $1 \times L$ vector defined as

$$[\alpha_f^{\text{FD}}]_i = \max([\mathbf{x}_1^{\text{FD}}]_i, [\mathbf{x}_2^{\text{FD}}]_i), \quad \forall i \in [1, L] \quad (48)$$

To this end, based on the above and assuming that problem PC – FD is feasible, its optimal solution is given in the following theorem.

Theorem 4. Assuming that problem PC – FD is feasible, i.e., conditions (42a) and (42b) hold, its optimal solution is given by

$$(\alpha_n^{\text{FD}*}, \alpha_f^{\text{FD}*}, \beta^{\text{FD}*}) = \underset{\mathbf{p}^{\text{FD}} \in \mathcal{P}^{\text{FD}}}{\operatorname{argmin}} f(\mathbf{p}^{\text{FD}}), \quad (49)$$

where $\mathcal{P}^{\text{FD}} = \{\mathbf{p}_1^{\text{FD}}, \dots, \mathbf{p}_L^{\text{FD}}\}$, where for $i \in [1, L]$, \mathbf{p}_i^{FD} is the 1×3 vector expressed as $\mathbf{p}_i^{\text{FD}} = ([\alpha_n^{\text{FD}}]_i, [\alpha_f^{\text{FD}}]_i, [\beta^{\text{FD}}]_i)$.

Proof. See Appendix D. □

C. RIS-enabled FD C-NOMA: Phase-Shift Coefficients Optimization

Let $\mathbf{v} = [v_1, \dots, v_M]^H$, where for all $m \in \llbracket 1, M \rrbracket$, $v_m = e^{j\theta_m}$. By applying the change of variables $\mathbf{h}_{\text{rn}}^H \Theta^{\text{FD}} \mathbf{h}_{\text{br}} = \mathbf{v}^H \Phi$, where $\Phi = \text{diag}(\mathbf{h}_{\text{rn}}^H) \mathbf{h}_{\text{br}} \in \mathbb{C}^{M \times 1}$, $\mathbf{h}_{\text{rf}}^H \Theta^{\text{FD}} \mathbf{h}_{\text{br}} = \mathbf{v}^H \Psi$, where $\Psi = \text{diag}(\mathbf{h}_{\text{rf}}^H) \mathbf{h}_{\text{br}} \in \mathbb{C}^{M \times 1}$, and $\mathbf{h}_{\text{rf}}^H \Theta^{\text{FD}} \mathbf{h}_{\text{nr}} = \mathbf{v}^H \Xi$, where $\Xi = \text{diag}(\mathbf{h}_{\text{rf}}^H) \mathbf{h}_{\text{nr}} \in \mathbb{C}^{M \times 1}$, we have

$$\begin{aligned} |h_{\text{bn}} + \mathbf{h}_{\text{rn}}^H \Theta^{\text{FD}} \mathbf{h}_{\text{br}}|^2 &= |h_{\text{bn}} + \mathbf{v}^H \Phi|^2, \\ |h_{\text{bf}} + \mathbf{h}_{\text{rf}}^H \Theta^{\text{FD}} \mathbf{h}_{\text{br}}|^2 &= |h_{\text{bf}} + \mathbf{v}^H \Psi|^2, \\ |h_{\text{nf}} + \mathbf{h}_{\text{rf}}^H \Theta^{\text{FD}} \mathbf{h}_{\text{nr}}|^2 &= |h_{\text{nf}} + \mathbf{v}^H \Xi|^2. \end{aligned} \quad (50)$$

Then, the achievable data rates in (16), (17), and (19) can be expressed as follows

$$\mathcal{R}_{\text{n} \rightarrow \text{f}}^{\text{FD}} = \log \left(1 + \frac{\alpha_{\text{f}}^{\text{FD}} P_{\text{BS}} (\bar{\mathbf{v}}^H \mathbf{Q}_{\text{bn}} \bar{\mathbf{v}} + |h_{\text{bn}}|^2)}{\alpha_{\text{n}}^{\text{FD}} P_{\text{BS}} (\bar{\mathbf{v}}^H \mathbf{Q}_{\text{bn}} \bar{\mathbf{v}} + |h_{\text{bn}}|^2) + \beta^{\text{FD}} P_{\text{n}} \gamma_{\text{SI}} + \sigma_{\text{n}}^2} \right), \quad (51)$$

$$\mathcal{R}_{\text{n} \rightarrow \text{n}}^{\text{FD}} = \log \left(1 + \frac{\alpha_{\text{n}}^{\text{FD}} P_{\text{BS}} (\bar{\mathbf{v}}^H \mathbf{Q}_{\text{bn}} \bar{\mathbf{v}} + |h_{\text{bn}}|^2)}{\beta^{\text{FD}} P_{\text{n}} \gamma_{\text{SI}} + \sigma_{\text{n}}^2} \right), \quad (52)$$

$$\mathcal{R}_{\text{MRC}}^{\text{FD}} = \log \left(1 + \frac{\alpha_{\text{f}}^{\text{FD}} P_{\text{BS}} (\bar{\mathbf{v}}^H \mathbf{Q}_{\text{bf}} \bar{\mathbf{v}} + |h_{\text{bf}}|^2) + \beta^{\text{FD}} P_{\text{n}} (\bar{\mathbf{v}}^H \mathbf{Q}_{\text{nf}} \bar{\mathbf{v}} + |h_{\text{nf}}|^2)}{\alpha_{\text{n}}^{\text{FD}} P_{\text{BS}} (\bar{\mathbf{v}}^H \mathbf{Q}_{\text{bf}} \bar{\mathbf{v}} + |h_{\text{bf}}|^2) + 1} \right), \quad (53)$$

where

$$\mathbf{Q}_{\text{bn}} = \begin{bmatrix} \Phi \Phi^H & \Phi h_{\text{bn}}^H \\ h_{\text{bn}} \Phi^H & 0 \end{bmatrix}, \quad \mathbf{Q}_{\text{bf}} = \begin{bmatrix} \Psi \Psi^H & \Psi h_{\text{bf}}^H \\ h_{\text{bf}} \Psi^H & 0 \end{bmatrix}, \quad \mathbf{Q}_{\text{nf}} = \begin{bmatrix} \Xi \Xi^H & \Xi h_{\text{nf}}^H \\ h_{\text{nf}} \Xi^H & 0 \end{bmatrix}, \quad \bar{\mathbf{v}} = \begin{bmatrix} \mathbf{v} \\ t \end{bmatrix}. \quad (54)$$

Note that $\bar{\mathbf{v}}^H \mathbf{Q}_z \bar{\mathbf{v}} = \text{tr}(\mathbf{Q}_z \bar{\mathbf{v}} \bar{\mathbf{v}}^H)$ for all $k \in \{\text{bn}, \text{bf}, \text{nf}\}$ and define $\mathbf{V} = \bar{\mathbf{v}} \bar{\mathbf{v}}^H$, which needs to satisfy $\text{rank}(\mathbf{V}) = 1$ and $\mathbf{V} \succeq 0$. However, the rank-one constraint is non-convex [36]. By relaxing this constraint, the optimization problem PS – FD can be transformed into

$$\hat{\mathcal{P}} : \text{Find } \boldsymbol{\theta}^{\text{FD}}, \quad (55\text{a})$$

$$\text{s.t. } \alpha_{\text{n}}^{\text{FD}} P_{\text{BS}} (\text{tr}(\mathbf{Q}_{\text{bn}} \mathbf{V}) + |h_{\text{bn}}|^2) \geq t_{\text{n}}^{\text{FD}} (\beta^{\text{FD}} P_{\text{n}} \gamma_{\text{SI}} + \sigma_{\text{n}}^2), \quad (55\text{b})$$

$$\text{tr}(\mathbf{Q} \mathbf{V}) + \alpha_{\text{f}}^{\text{FD}} P_{\text{BS}} |h_{\text{bf}}|^2 + \beta^{\text{FD}} P_{\text{n}} |h_{\text{nf}}|^2 \geq t_{\text{f}}^{\text{FD}} (\alpha_{\text{n}}^{\text{FD}} P_{\text{BS}} (\text{tr}(\mathbf{Q}_{\text{bf}} \mathbf{V}) + |h_{\text{bf}}|^2) + \sigma_{\text{f}}^2), \quad (55\text{c})$$

$$\alpha_{\text{f}}^{\text{FD}} P_{\text{BS}} (\text{tr}(\mathbf{Q}_{\text{bn}} \mathbf{V}) + |h_{\text{bn}}|^2) \geq t_{\text{f}}^{\text{FD}} (\alpha_{\text{n}}^{\text{FD}} P_{\text{BS}} (\text{tr}(\mathbf{Q}_{\text{bn}} \mathbf{V}) + |h_{\text{bn}}|^2) + \beta^{\text{FD}} P_{\text{n}} \gamma_{\text{SI}} + \sigma_{\text{f}}^2), \quad (55\text{d})$$

$$\mathbf{V} \succeq 0, \quad (55\text{e})$$

$$[\mathbf{V}]_{m,m} = 1, \quad \forall m \in \llbracket 1, M+1 \rrbracket, \quad (55\text{f})$$

where $\mathbf{Q} = \alpha_{\text{f}}^{\text{FD}} P_{\text{BS}} \mathbf{Q}_{\text{bf}} + \beta^{\text{FD}} P_{\text{n}} \mathbf{Q}_{\text{nf}}$. It is not difficult to observe that problem $\hat{\mathcal{P}}$ is an SDP. Thus, an optimal solution can be obtained by existing convex optimization solvers such as CVX [36]. However,

due to the rank one constraint relaxation, the SDR may not be tight for PS – FD. To overcome this issue, the Gaussian randomization approach can be similarly used to find a feasible solution to problem PS – FD dependent on the higher-rank solution that is obtained by solving problem $\hat{\mathcal{P}}$. Following the same procedures in **Algorithm 1**, the solutions for the phase-shift coefficients, θ^{FD} , and the power control coefficients, $(\alpha_n^{\text{FD}}, \alpha_f^{\text{FD}}, \beta^{\text{FD}})$ can be obtained.

VI. RESULTS AND DISCUSSION

In this section, several numerical examples and simulation results are presented to examine the performance of the proposed schemes RIS-enabled FD C-NOMA and RIS-enabled HD C-NOMA networks. Since it has been proven that the performance of traditional FD C-NOMA has better performance than the HD C-NOMA counterpart, we consider the traditional FD C-NOMA technique without any assistance of RIS as a benchmark [30], [38], [39]. This technique is referred to as "FD C-NOMA without RIS". In this scheme, the BS communicates with UE_n and UE_f and UE_n communication with UE_f in the same time-slot without any aid from the RIS. Hence, with the same target objective (power consumption minimization), we only need to use the power allocation coefficients at the BS and UE_n to minimize the total transmit power, which are obtained by **Theorem 4** considering only the direct channel gains (BS \rightarrow UE_n , BS \rightarrow UE_f , and $\text{UE}_n \rightarrow$ UE_f) in the derived closed-form expressions.

A. Simulation Settings

The simulation environment consists of one BS, one RIS, one UE_n , and one UE_f which are located in a 3-dimensional Cartesian coordinates systems (X, Y, Z) at $(0 \text{ m}, 10 \text{ m}, 0 \text{ m})$, $(80 \text{ m}, 10 \text{ m}, 0 \text{ m})$, $(40 \text{ m}, 0 \text{ m}, 0 \text{ m})$ and $(80 \text{ m}, 0 \text{ m}, 0 \text{ m})$, respectively. Note that the RIS is located nearby UE_f to enhance its communication link and correspondingly its achievable data rate, which reflects on minimizing the required transmission power. Moreover, the SI at UE_n is modeled as a Rayleigh fading with zero mean and Ω_{SI} variance [31]. Note that, Monte-Carlo simulations are employed over 10^4 independent channel realizations. The system parameters for the simulations are listed in Table II [17], [27], [40].

B. Convergence of The Proposed Schemes

Fig. 2 describes the convergence behavior of the proposed RIS-enabled FD C-NOMA and RIS-enabled HD C-NOMA algorithms versus the iteration number with number of RIS elements $M = 80$, SI parameter $\Omega_{\text{SI}} = -100$ dB, and minimum required rate for UE_f $R_f^{\text{th}} = 2$ bits/sec/Hz. It can be observed that the proposed RIS-enabled FD C-NOMA and RIS-enabled HD C-NOMA algorithms converge in about 4 to 5 iterations, which provides a low computational complexity [36].

TABLE II
SIMULATION PARAMETERS

Parameter	Symbol	Value
Rician factors of the BS-RIS and the RIS-UE _f links	κ_{br}, κ_{rf}	3 dB
Path-loss at reference distance of 1 m	ρ_0	-30 dB
Path-loss exponents for the BS-RIS and for the RIS-UE _f links	η_{br}, η_{rf}	2.2
Path-loss exponents for the BS-UE _f and for the UE _n -UE _f links	η_{bf}, η_{nf}	4
Path-loss exponent for the BS-UE _n link	η_{bn}	3.5
Path-loss exponent for the UE _n -RIS link	η_{nr}	3
Power budget at the BS	P_{BS}	33 dBm
Power budget at UE _n	P_n	23 dBm
Noise power at UE _n and UE _f	σ_n^2, σ_f^2	-90 dB
Minimum rate QoS requirement for UE _n	R_n^{th}	1 bits/sec/Hz

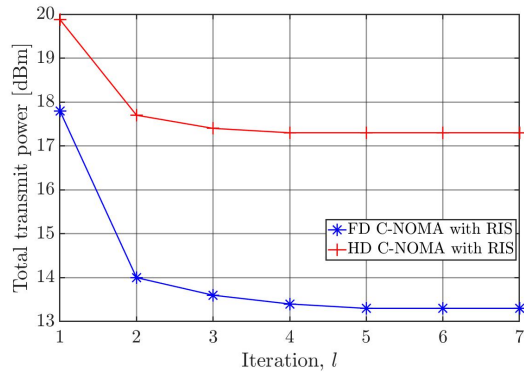


Fig. 2. Convergence of the proposed algorithm.

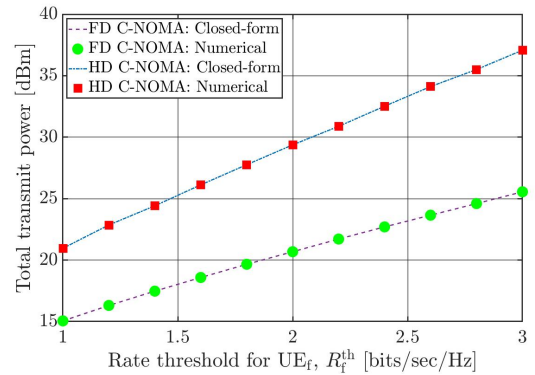


Fig. 3. Analytical and numerical total transmit power versus the rate threshold for UE_f.

C. Validation of The Closed-form Expressions for The Power Allocation Coefficients

It can be seen that the closed-form expressions in **Theorem 2** and **Theorem 4** are derived for a given phase-shift matrix. As a result, in order to validate the closed-form expression for the power allocation coefficients, we consider FD C-NOMA without RIS and HD- C-NOMA without RIS as the schemes that validate the analytical results. Fig. 3 depicts the analytical and numerical total transmit power for FD C-NOMA without RIS and HD C-NOMA without RIS schemes versus the minimum required rate for UE_f, R_f^{th} with $\Omega_{SI} = -90$ dB. The analytical results are obtained based on the closed-form expressions derived in **Theorem 2** and **Theorem 4**, while the numerical results are obtained by solving problem PC – HD and PC – FD using an off-the-shelf optimization solver.

³ It can be seen from Fig. 3 that the analytical results match perfectly the numerical results which

³The adopted solver is fmincon that is a predefined MATLAB solver [10], [30], [41]. Moreover, 10^3 different initial points are generated to guarantee the convergence of the solver to the optimal solution.

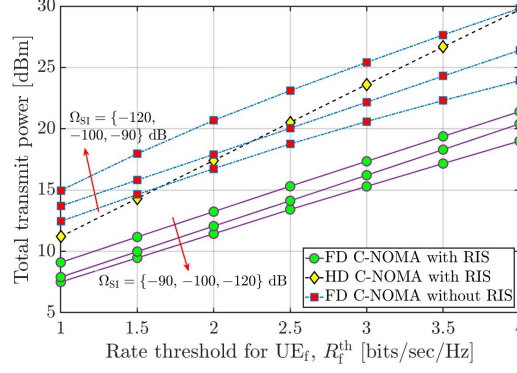


Fig. 4. Total transmit power versus the rate threshold R_f^{th} of UE_f with different SI values due to the FD operation ($M = 80$).

validates the optimality of the closed-form expressions of the power allocation coefficients obtained by *Theorem 2* and *Theorem 4*.

D. Total Transmit Power Performance

Fig. 4 compares the performance of the proposed RIS-enabled FD C-NOMA scheme, the proposed RIS-enabled HD C-NOMA, and the FD C-NOMA without RIS adopted in [34], [38], [39], when varying the required data rate threshold for UE_f . Different values of the SI channel gain parameter Ω_{SI} are considered for the cases of RIS-enabled FD C-NOMA and FD C-NOMA without RIS schemes. First, it can be seen that FD C-NOMA with RIS scheme has a significant gain compared to HD C-NOMA with RIS and FD C-NOMA without RIS. Second, due to the pre-log penalty in the HD scenario, the gap between the FD C-NOMA with RIS and the HD C-NOMA with RIS increases when the required data rate threshold increases. Third, since the RIS constructs strong combined channel gain for the BS- UE_f and UE_n - UE_f communication links, this makes the active nodes (BS and UE_n) able to transmit with low power, and hence, the effects of the SI on the system performance is weak compared to the FD C-NOMA without RIS. Finally, it can be seen that the HD C-NOMA with RIS has the ability to beat the FD C-NOMA without RIS proposed in [34], [38], [39]. Depending on the strength of the SI, the HD C-NOMA with RIS can achieve a better performance for most of the considered cases (different rate thresholds for UE_f).

Fig. 5 presents the total transmit power for the three schemes versus the number of RIS reflecting elements, and $\Omega_{\text{SI}} = -100$ dB, where the rate QoS constraint at UE_f $R_f^{\text{th}} = 2$ bits/s/Hz in Fig. 5.a and $R_f^{\text{th}} = 3$ bits/s/Hz in Fig. 5.b. First, it is observed that the total transmit power that is required by the RIS-based schemes decreases when the number of meta-atoms of the RIS increases while the total

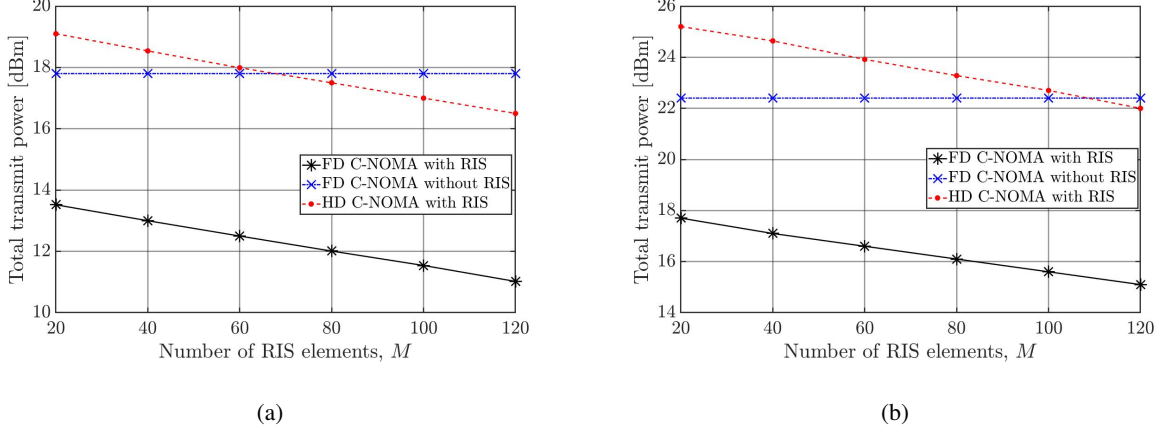


Fig. 5. Total transmit power versus the number of RIS elements, when $\Omega_{SI} = -100$ dB, where (a) for the case when $R_f^{\text{th}} = 2$ bits/s/Hz and (b) for the case when $R_f^{\text{th}} = 3$ bits/s/Hz.

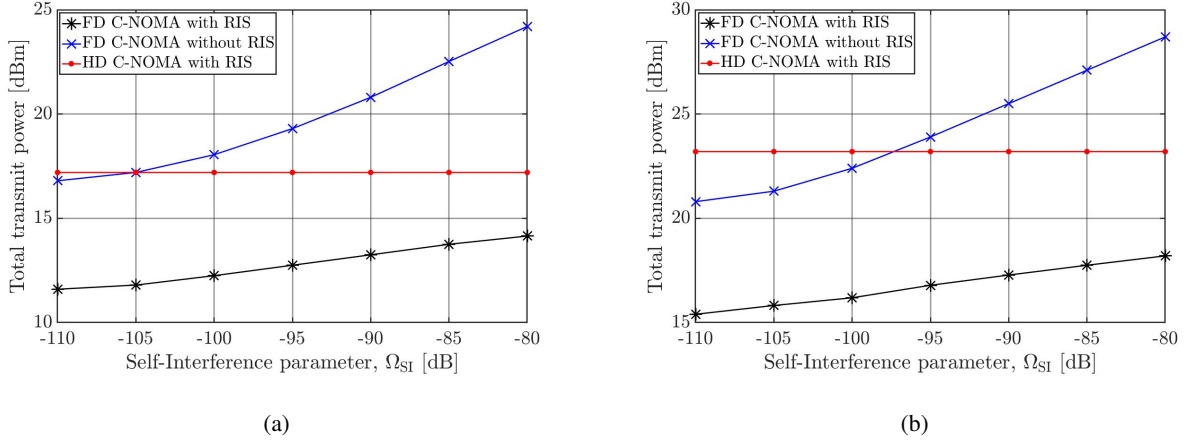


Fig. 6. Total transmit power versus the SI parameter at UE_n , when the number of reflecting elements at the RIS is $M = 80$ dB, where (a) for the case when $R_f^{\text{th}} = 2$ bits/s/Hz and (b) for the case when $R_f^{\text{th}} = 3$ bits/s/Hz.

transmit power for FD C-NOMA without RIS scheme remains unchanged. This is because a larger number of RIS meta-atoms leads to a higher combined channel gains and hence a higher passive array gains. Second, it can be seen that the number of meta-atoms required at the RIS to allow the HD C-NOMA with RIS to beat the traditional FD C-NOMA depends on the required QoS at UE_f . This is because a high QoS requirement at UE_f needs a high passive array gain to overcome the pre-log penalty in the HD mode. Third, the RIS-enabled FD C-NOMA network significantly outperforms the other schemes, which reveals the potential of integrating RIS in FD C-NOMA networks in enhancing the network power efficiency.

Fig. 6.a and Fig. 6.b depict the total transmit power versus the SI values at the near NOMA user

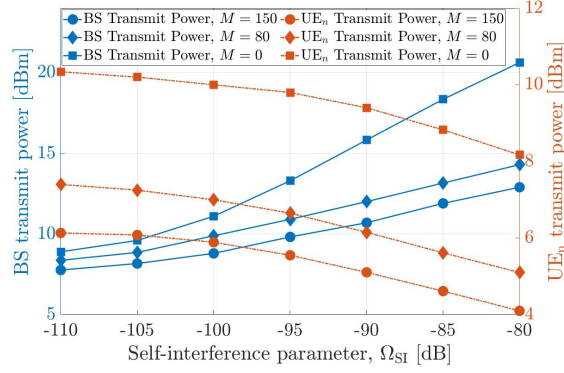


Fig. 7. Total transmit power by the BS and UE_n versus the SI channel gains with different number of RIS elements for the proposed FD C-NOMA with RIS.

for $R_f^{\text{th}} = 2$ and $R_f^{\text{th}} = 3$, respectively, when $M = 80$. First, it can be observed that the proposed FD C-NOMA with RIS scheme gives a significant performance enhancement than the HD C-NOMA with RIS scheme when Ω_{SI} is relatively small. However, as Ω_{SI} increases, the performance gain between them decreases. This is because increasing the SI value restricts the power transmission at UE_n and hence the BS should increase its transmit power in order to meet the QoS constraint at UE_f. Second, the HD C-NOMA with RIS scheme can achieve a significant performance compared to FD C-NOMA without RIS when Ω_{SI} increases. This is because increasing Ω_{SI} leads to deteriorating the performance of the FD mode and hence the passive array gain at the RIS can make the HD C-NOMA with RIS be a favorable scheme compared to the FD C-NOMA without RIS scheme. Third, it can be also observed that the total transmit power in the network without RIS is sharply increasing in comparison with the rate of increase in the network with RIS. This means that the system with RIS can tolerate high values of SI, which validates the effectiveness of the amalgamation between FD C-NOMA and RIS.

Fig. 7 shows the effect of increasing the SI on the transmit power at both the BS and the near NOMA user for different numbers of RIS elements. It can be seen that the RIS elements have a great impact on the amount of transmit power at the active nodes (BS and UE_n). In addition, it can be also seen that when Ω_{SI} increases, UE_n should reduce its transmit power to avoid degrading its performance. On the other hand, reducing the power at UE_n will lead to a sharp increase at the BS side, which shed the lights on the effect of the D2D communication on the network performance in terms of the power efficiency. For instance, for $M = 80$, when Ω_{SI} increases from -100 dB to -90 dB, the transmit power at UE_n reduces by 0.9 dB, whereas the transmit power at the BS increases by 3 dB.

VII. CONCLUSION

In this paper, we investigated the RIS-empowered HD/FD C-NOMA downlink transmission scheme in order to minimize the total transmit power at the BS and at the relay user by jointly optimizing the power allocation coefficients at the BS and the transmit relaying power at the near NOMA user, along with the phase-shift coefficients at the RIS. In this formulated problem, we considered the QoS requirements in terms of the minimum data rate, SIC constraint, the power budget at the BS and the near NOMA user, and the RIS elements constraints. By invoking the alternating optimization technique, the non-convex power minimization optimization problem is decomposed into two sub-problems, power allocation optimization sub-problem and phase-shift optimization sub-problem, which are solved in an alternate manner. By leveraging the SDR, the RIS phase-shift coefficients are obtained. Meanwhile, for the power allocation sub-problem, we derived closed-form expressions for the optimal power allocation coefficients at the BS and the optimal transmit-relaying power from the near NOMA user. The Simulation results show that the proposed RIS-enabled FD C-NOMA scheme significantly outperforms the FD C-NOMA without the assistance of the RIS. In addition, in spite of the pre-log penalty in the HD relaying mode, and according to the required QoS at the far NOMA user, the number of reflecting elements and the SI value, the proposed RIS-enabled HD C-NOMA can outperform the FD C-NOMA without RIS.

APPENDIX A

PROOF OF THEOREM 1

In this section, we present the proof of *Theorem 1*. At the beginning, constraints (21b)-(21g) can be expressed as

$$0 \leq \alpha_n^{\text{HD}} \leq \alpha_f^{\text{HD}} \leq 1, \quad (56a)$$

$$\alpha_f^{\text{HD}} \leq 1 - \alpha_n^{\text{HD}}, \quad (56b)$$

$$0 \leq \beta^{\text{HD}} \leq 1, \quad (56c)$$

$$\alpha_n^{\text{HD}} \geq \frac{t_n^{\text{HD}}}{\gamma_{\text{bn}}}, \quad (56d)$$

$$\alpha_f^{\text{HD}} \geq \alpha_n^{\text{HD}} t_f^{\text{HD}} + \frac{t_f^{\text{HD}}}{\gamma_{\text{bn}}}, \quad (56e)$$

$$\beta^{\text{HD}} \geq \frac{t_f^{\text{HD}}}{\gamma_d} - \frac{\alpha_f^{\text{HD}} \gamma_{\text{bf}}}{\gamma_d (\alpha_n^{\text{HD}} \gamma_{\text{bf}} + 1)}. \quad (56f)$$

Constraints (56a) and (56b) imply $0 \leq \alpha_n^{\text{HD}} \leq \frac{1}{2}$. In addition, constraints (56b) and (56e) imply $\alpha_n^{\text{HD}} \leq \frac{\gamma_{\text{bn}} - t_f^{\text{HD}}}{\gamma_{\text{bn}}(t_f^{\text{HD}} + 1)}$. Therefore, it can be concluded that α_n^{HD} should satisfy $\alpha_{\text{min}}^{\text{HD}} \leq \alpha_n^{\text{HD}} \leq \alpha_{\text{max}}^{\text{HD}}$,

where $\alpha_{\min}^{\text{HD}}$ and $\alpha_{\max}^{\text{HD}}$ are expressed as shown in (26) in **Theorem 1**. Hence, for problem PC – HD to be feasible, the condition $\alpha_{\min}^{\text{HD}} \leq \alpha_{\max}^{\text{HD}}$ should be satisfied. On the other hand, one can remark that the lowest value of β^{HD} that satisfies constraint (56f) is reached at the lowest feasible value of α_n^{HD} and the highest feasible value of α_f^{HD} . In this context, based on constraint (56d), the lowest feasible value of α_n^{HD} is $\alpha_n^{\text{HD}} = \alpha_{\min}^{\text{HD}} = \frac{t^{\text{HD}}}{\gamma_{\text{bn}}}$ and, based on constraint (56b), the highest feasible value of α_f^{HD} is $\alpha_n^{\text{HD}} = 1 - \alpha_{\min}^{\text{HD}} = 1 - \frac{t^{\text{HD}}}{\gamma_{\text{bn}}}$. Therefore, the lowest feasible value of β^{HD} is given by β_{\min}^{HD} in (26). Consequently, for problem PC – HD to be feasible, the condition $\beta_{\min}^{\text{HD}} \leq \beta_{\max}^{\text{HD}}$ should be also satisfied, where $\beta_{\max}^{\text{HD}} = 1$, which completes the proof.

APPENDIX B

PROOF OF THEOREM 2

In this section, we present the proof of **Theorem 2**. With the goal of minimizing the total transmit power of the C-NOMA cellular system, two directions can be considered. The first direction consists of minimizing the BS transmit power first and then minimizing the one of the near UE, while the second direction consists of minimizing the transmit power of the near UE first and then minimizing the one of the BS. Let us start with the first direction. As discussed in the previous appendix, the lowest feasible value of α_n^{HD} is $\alpha_{n,1}^{\text{HD}} = \alpha_{\min}^{\text{HD}}$. Based on this, we can see from constraints (56a) and (56e) that the lowest feasible value of α_f^{HD} is $\alpha_{f,1}^{\text{HD}} = \max\left(\alpha_{\min}^{\text{HD}}, \alpha_{\min}^{\text{HD}} t_f^{\text{HD}} + \frac{t_f^{\text{HD}}}{\gamma_n}\right)$. Therefore, by injecting these two values in constraint (56f), we conclude that the lowest value of β^{HD} is $\beta_1^{\text{HD}} = \frac{1}{\gamma_d} \left(t_f^{\text{HD}} - \frac{\alpha_{f,1}^{\text{HD}} \gamma_f}{\alpha_{n,1}^{\text{HD}} \gamma_f + 1} \right)$. Now, considering the second direction, the lowest feasible value of β^{HD} is $\beta_1^{\text{HD}} = 0$. on the other hand, recall that the lowest feasible value of α_n^{HD} is $\alpha_{n,2}^{\text{HD}} = \alpha_{\min}^{\text{HD}}$. Therefore, by injecting these two values in constraint (56f), we find that the lowest feasible value of α_f^{HD} is $\alpha_{f,2}^{\text{HD}} = \frac{(\alpha_{\min}^{\text{HD}} \gamma_{\text{bn}} + 1) t_f^{\text{HD}}}{\gamma_{\text{bn}}}$. Finally, the optimal power control scheme is the one among the above two schemes that minimize the total transmit power of the HD C-NOMA system, which completes the proof.

APPENDIX C

PROOF OF THEOREM 3

In this section, we present the proof of **Theorem 3**. At the beginning, constraints (38b)-(38g) can be expressed as

$$0 \leq \alpha_n^{\text{FD}} \leq \alpha_f^{\text{FD}} \leq 1, \quad (57a)$$

$$\alpha_f^{\text{FD}} \leq 1 - \alpha_n^{\text{FD}}, \quad (57b)$$

$$0 \leq \beta^{\text{FD}} \leq 1, \quad (57c)$$

$$\alpha_n^{\text{FD}} \geq \frac{\gamma_{\text{SI}}}{\gamma_{\text{bn}}} \beta^{\text{FD}} + \frac{t_n^{\text{FD}}}{\gamma_{\text{bn}}}, \quad (57\text{d})$$

$$\alpha_f^{\text{FD}} \geq \alpha_n^{\text{FD}} t_f^{\text{FD}} + \frac{\gamma_{\text{SI}} t_f^{\text{FD}}}{\gamma_{\text{bn}}} \beta^{\text{FD}} + \frac{t_f^{\text{FD}}}{\gamma_{\text{bn}}}, \quad (57\text{e})$$

$$\alpha_f^{\text{FD}} \geq \alpha_n^{\text{FD}} t_f^{\text{FD}} - \frac{\gamma_d t_f^{\text{FD}}}{\gamma_{\text{bf}}} \beta^{\text{FD}} + \frac{t_f^{\text{FD}}}{\gamma_{\text{bf}}}. \quad (57\text{f})$$

Constraints (57a) and (57b) imply $0 \leq \alpha_n^{\text{FD}} \leq \frac{1}{2}$. Let B_1 be the bound whose expression is given in constraint (57d). In addition, constraints (57b) and (57e) imply

$$B_2 : \alpha_n^{\text{HD}} \leq \frac{\gamma_{\text{bn}} - t_f^{\text{HD}} - P_n \gamma_{\text{SI}} t_f^{\text{HD}} \beta^{\text{FD}}}{\gamma_{\text{bn}} (t_f^{\text{HD}} + 1)}. \quad (58)$$

Moreover, based on constraints (57b) and (57f), we obtain

$$B_3 : \alpha_n^{\text{HD}} \leq \frac{\gamma_{\text{bn}} - t_f^{\text{HD}} + P_n \gamma_d \beta^{\text{FD}}}{\gamma_{\text{bf}} (t_f^{\text{HD}} + 1)}. \quad (59)$$

The bounds B_1 , B_2 and B_3 are, each, a function of the variables $(\alpha_n^{\text{FD}}, \beta^{\text{FD}})$. Therefore, problem PC – FD is feasible if and only if the bound B_1 can be lower than the bounds B_2 and B_3 simultaneously within the region $(\alpha_n^{\text{FD}}, \beta^{\text{FD}}) \in [0, \frac{1}{2}] \times [0, 1]$. The condition $B_1 \leq B_2$ implies that β^{FD} should satisfy $\beta^{\text{FD}} \leq \frac{\gamma_n - t_f^{\text{FD}} - t_n^{\text{FD}} (1 + t_f^{\text{FD}})}{\gamma_{\text{SI}} t_n^{\text{FD}} (1 + t_f^{\text{FD}}) + t_f^{\text{FD}}}$. On the other hand, the condition $B_1 \leq B_3$ implies that β^{FD} should satisfy $\beta^{\text{FD}} \geq \frac{\gamma_{\text{bf}} - t_f^{\text{FD}} - \frac{\gamma_{\text{bf}} (1 + t_f^{\text{FD}}) t_n^{\text{FD}}}{\gamma_n}}{c_1 - c_2}$ if $c_1 \leq c_2$ and $\beta^{\text{FD}} \leq \frac{\gamma_{\text{bf}} - t_f^{\text{FD}} - \frac{\gamma_{\text{bf}} (1 + t_f^{\text{FD}}) t_n^{\text{FD}}}{\gamma_n}}{c_1 - c_2}$ if $c_1 \geq c_2$. Therefore, along with the fact that $\beta^{\text{FD}} \in [0, 1]$, we obtain the first condition in **Theorem 3**. Furthermore, since B_1 should be lower than the bounds B_2 and B_3 simultaneously within the region $(\alpha_n^{\text{FD}}, \beta^{\text{FD}}) \in [0, \frac{1}{2}] \times [0, 1]$, we conclude that $\frac{\gamma_{\text{SI}} t_n^{\text{FD}}}{\gamma_{\text{bn}}} \beta_{\text{min}}^{\text{FD}} + \frac{t_n^{\text{FD}}}{\gamma_{\text{bn}}}$ should be lower than $\frac{1}{2}$, which is the second condition of **Theorem 3** and this completes the proof.

APPENDIX D

PROOF OF THEOREM 4

In this section, we present the proof of **Theorem 4**. Since the objective function of problem PC – FD, the optimal solution is one of the intersection points of the boundaries of its feasibility region. The point with coordinates $(\alpha_c^{\text{FD}}, \beta_c^{\text{FD}})$, defined in (45) represents the intersection point of the bounds B_2 and B_3 . Therefore, depending on whether β_c^{FD} is within the feasibility interval $[\beta_{\text{min}}^{\text{FD}}, \beta_{\text{max}}^{\text{FD}}]$, this intersection point is transformed into the point $(\alpha_0^{\text{FD}}, \beta_0^{\text{FD}})$ in (46) in order to verify if this point should be considered as a candidate solutions or no. Based on this, the intersection points of the the boundaries of the feasibility region of problem PC – FD are given in (47). Afterwards, for each intersection point $(\alpha_n^{\text{FD}}, \beta^{\text{FD}})$, the corresponding α_f^{FD} can be obtained as shown in (48), which in turn constructs a candidate solution $(\alpha_n^{\text{FD}}, \alpha_f^{\text{FD}}, \beta^{\text{FD}})$. Consequently, the optimal solution of problem

PC – FD is the candidate solution that produces the lowest objective function as presented in **Theorem 4**, which completes the proof.

REFERENCES

- [1] M. Vaezi *et al.*, “Interplay between NOMA and other emerging technologies: A survey,” *IEEE Trans. Cogn. Commun. Netw.*, vol. 5, no. 4, pp. 900–919, 2019.
- [2] I. F. Akyildiz, A. Kak, and S. Nie, “6G and beyond: The future of wireless communications systems,” *IEEE Access*, vol. 8, pp. 133 995 – 134 030, Jul. 2020.
- [3] Z. Ding, X. Lei, G. K. Karagiannidis, R. Schober, J. Yuan, and V. K. Bhargava, “A survey on non-orthogonal multiple access for 5g networks: Research challenges and future trends,” *IEEE J. Sel. Areas Commun.*, vol. 35, no. 10, pp. 2181–2195, 2017.
- [4] M. Elhattab *et al.*, “CoMP transmission in downlink NOMA-based heterogeneous cloud radio access networks,” *IEEE Trans. Commun.*, 2020.
- [5] Z. Ding and H. Poor, “A simple design of IRS-NOMA transmission,” *IEEE Commun. Lett.*, vol. 24, no. 5, pp. 1119–1123, 2020.
- [6] Z. Zhang, H. Sun, and R. Q. Hu, “Downlink and uplink non-orthogonal multiple access in a dense wireless network,” *IEEE J. Sel. Areas Commun.*, vol. 35, no. 12, pp. 2771–2784, 2017.
- [7] Y. Liu, Z. Qin, M. Elkashlan, A. Nallanathan, and J. A. McCann, “Non-orthogonal multiple access in large-scale heterogeneous networks,” *IEEE J. Sel. Areas Commun.*, vol. 35, no. 12, pp. 2667–2680, 2017.
- [8] M. Zeng *et al.*, “Cooperative NOMA: State of the art, key techniques, and open challenges,” *IEEE Network*, vol. 34, no. 5, pp. 205–211, 2020.
- [9] M. Elhattab, M. A. Arfaoui, and C. Assi, “A joint CoMP C-NOMA for enhanced cellular system performance,” *IEEE Communications Letters*, vol. 24, no. 9, pp. 1919–1923, 2020.
- [10] M. Elhattab *et al.*, “Power allocation in CoMP-empowered C-NOMA networks,” *IEEE Networking Letters*, pp. 1–1, 2020.
- [11] A. Sena *et al.*, “What role do intelligent reflecting surfaces play in multi-antenna non-orthogonal multiple access?” *IEEE Wireless Commun.*, vol. 27, no. 5, pp. 24–31, 2020.
- [12] S. Gonget *et al.*, “Towards smart wireless communications via intelligent reflecting surfaces: A contemporary survey,” *IEEE Commun. Surveys Tuts.*, pp. 1–1, 2020.
- [13] E. Basar *et al.*, “Wireless communications through reconfigurable intelligent surfaces,” *IEEE Access*, vol. 7, pp. 116 753–116 773, Aug. 2019.
- [14] B. Zheng, Q. Wu, and R. Zhang, “Intelligent reflecting surface-assisted multiple access with user pairing: NOMA or OMA?” *IEEE Commun. Lett.*, vol. 24, no. 4, pp. 753–757, 2020.
- [15] H. Wang, C. Liu, Z. Shi, Y. Fu, and R. Song, “On power minimization for IRS-aided downlink NOMA systems,” *IEEE Wireless Commun. Lett.*, vol. 9, no. 11, pp. 1808–1811, 2020.
- [16] M. Fu, Y. Zhou, Y. Shi, and K. B. Letaief, “Reconfigurable intelligent surface empowered downlink non-orthogonal multiple access,” [Online]. Available: <https://arxiv.org/abs/1910.07361>, 2020.
- [17] Y. Guo *et al.*, “Intelligent reflecting surface aided multiple access over fading channels,” *IEEE Trans. Commun.*, pp. 1–1, 2020.
- [18] X. Mu, Y. Liu, L. Guo, J. Lin, and N. Al-Dhahir, “Exploiting intelligent reflecting surfaces in NOMA networks: Joint beamforming optimization,” *IEEE Trans. Wireless Commun.*, vol. 19, no. 10, pp. 6884–6898, 2020.
- [19] W. Ni *et al.*, “Resource allocation for multi-cell IRS-aided NOMA networks,” [Online]. Available: <https://arxiv.org/abs/2006.11811>, 2020.
- [20] F. Fang, Y. Xu, Q. V. Pham, and Z. Ding, “Energy-efficient design of IRS-NOMA networks,” *IEEE Trans. Veh. Technol.*, vol. 69, no. 11, pp. 14 088–14 092, 2020.

- [21] G. Yang, X. Xu, and Y.-C. Liang, "Intelligent reflecting surface assisted non-orthogonal multiple access," [Online]. Available: <https://arxiv.org/abs/1907.03133v2>, 2020.
- [22] Z. Zhang, L. Lv, Q. Wu, H. Deng, and J. Chen, "Robust and secure communications in intelligent reflecting surface assisted NOMA networks," *IEEE Commun. Lett.*, pp. 1–1, 2020.
- [23] M. Elhattab, M. A. Arfaoui, C. Assi, and A. Ghayeb, "Reconfigurable intelligent surface assisted coordinated multipoint in downlink NOMA networks," *IEEE Commun. Lett.*, pp. 1–1, 2020.
- [24] T. Hou, Y. Liu, Z. Song, X. Sun, Y. Chen, and L. Hanzo, "Reconfigurable intelligent surface aided NOMA networks," *IEEE J. Sel. Areas Commun.*, vol. 38, no. 11, pp. 2575–2588, 2020.
- [25] Z. Ding and H. Poor, "A simple design of IRS-NOMA transmission," *IEEE Commun. Lett.*, vol. 24, no. 5, pp. 1119–1123, 2020.
- [26] C. Zhang, W. Yi, and Y. Liu, "Reconfigurable intelligent surfaces aided multi-cell NOMA networks: A stochastic geometry model," [Online]. Available: <https://arxiv.org/abs/2008.08457>, 2020.
- [27] J. Zuo, Y. Liu, and N. Al-Dhahir, "Reconfigurable intelligent surface assisted cooperative non-orthogonal multiple access systems," [Online]. Available: <https://arxiv.org/abs/2011.08975>, 2020.
- [28] C. You, B. Zheng, and R. Zhang, "Channel estimation and passive beamforming for intelligent reflecting surface: Discrete phase shift and progressive refinement," *IEEE J. Sel. Areas Commun.*, vol. 38, no. 11, pp. 2604–2620, 2020.
- [29] A. Taha, M. Alrabeiah, and A. Alkhateeb, "Enabling large intelligent surfaces with compressive sensing and deep learning," *arXiv preprint arXiv:1904.10136*, 2019.
- [30] P. Dinhet *et al.*, "A low-complexity framework for joint user pairing and power control for cooperative NOMA in 5G and beyond cellular networks," *IEEE Trans. Commun.*, pp. 1–1, 2020.
- [31] G. Liu, X. Chen, Z. Ding, Z. Ma, and F. R. Yu, "Hybrid half-duplex/full-duplex cooperative non-orthogonal multiple access with transmit power adaptation," *IEEE Trans. Wireless Commun.*, vol. 17, no. 1, pp. 506–519, 2018.
- [32] Z. Zhang, Z. Ma, M. Xiao, Z. Ding, and P. Fan, "Full-duplex device-to-device-aided cooperative nonorthogonal multiple access," *IEEE Trans. Veh. Technol.*, vol. 66, no. 5, pp. 4467–4471, 2017.
- [33] Z. Wei, X. Zhu, S. Sun, J. Wang, and L. Hanzo, "Energy-efficient full-duplex cooperative nonorthogonal multiple access," *IEEE Trans. Veh. Technol.*, vol. 67, no. 10, pp. 10 123–10 128, 2018.
- [34] X. Zhang and F. Wang, "Resource allocation for wireless power transmission over full-duplex OFDMA/NOMA mobile wireless networks," *IEEE J. Sel. Areas Commun.*, vol. 37, no. 2, pp. 327–344, 2019.
- [35] E. Bjornson, O. Ozdogan, and E. G. Larsson, "Intelligent reflecting surface versus decode-and-forward: How large surfaces are needed to beat relaying?" *IEEE Wireless Commun. Lett.*, vol. 9, no. 2, pp. 244–248, 2020.
- [36] Q. Wu and R. Zhang, "Intelligent reflecting surface enhanced wireless network via joint active and passive beamforming," *IEEE Trans. Wireless Commun.*, vol. 18, no. 11, pp. 5394–5409, 2019.
- [37] J. C. Bezdek and R. J. Hathaway, "Convergence of alternating optimization," *Neural, Parallel & Scientific Computations*, vol. 11, no. 4, pp. 351–368, 2003.
- [38] Z. Zhang, Z. Ma, M. Xiao, Z. Ding, and P. Fan, "Full-duplex device-to-device-aided cooperative nonorthogonal multiple access," *IEEE Trans. Veh. Technol.*, vol. 66, no. 5, pp. 4467–4471, 2017.
- [39] C. Zhong and Z. Zhang, "Non-orthogonal multiple access with cooperative full-duplex relaying," *IEEE Commun. Lett.*, vol. 20, no. 12, pp. 2478–2481, 2016.
- [40] M. Elhattab *et al.*, "Device-aware cell association in heterogeneous cellular networks: A matching game approach," *IEEE Trans. Green Commun. Net.*, vol. 3, no. 1, pp. 57–66, 2019.
- [41] S. Ebbesen, P. Kiwitz, and L. Guzzella, "A generic particle swarm optimization matlab function," in *2012 American Control Conference (ACC)*. IEEE, 2012, pp. 1519–1524.